An-Najah National University

Faculty of Graduate Studies

DEVELOPMENT OF NON-COVALENTLY FUNCTIONALIZED MULTIWALLED CARBON NANOTUBES BASED-SUBSTRATE FOR SUPPORTING IN VITRO NEURONAL GROWTH

By

Rama Sahem Hendawi

Supervisors

Dr. Naim Kittana

Dr. Mohyeddin Assali

This Thesis is submitted in Partial Fulfillment of the Requirements for the Degree of Master of Pharmacology, Faculty of Graduate Studies, An-Najah National University, Nablus – Palestine.

2023

DEVELOPMENT OF NON-COVALENTLY FUNCTIONALIZED MULTIWALLED CARBON NANOTUBES BASED-SUBSTRATE FOR SUPPORTING IN VITRO NEURONAL GROWTH

By

Rama Sahem Hendawi

This Thesis was Defended Successfully on 22/06/2023 and approved by

Dr. Naim Kittana Supervisor	Signature
Dr. Mohyddin Assali Co-Supervisor	Signature
Dr. Hussain Hallak External Examiner	Signature
Dr. Heba Salah Internal Examiner	Signature

Dedication

I dedicate this thesis, with every effort was made, and every difficult moment I had to deliver this work, to the people of my city Jenin, to every fighter for our freedom and dignity.

I would like to dedicate this work especially to the Six Gillboua fighters and their families, whom story inspired me and pushed me forward when I collapsed.

Acknowledgment

After thanking God for his endless blessings which surrounded me during my master journey, I would like to thank Palestinian German Science Bridge (PGSB) program for giving me the opportunity to complete the practical part of the thesis at Forschungzentrum Juelich (FZJ) IBI-2 institute.

I would like to deeply thank the group leader Dr. Bernd Hoffmann from IBI-2, in addition to supervisors from An-najah national university; Dr. Mohyeddin Assali, and Dr. Naim kittana for their support, motivation, immense knowledge, and for giving me this outstanding opportunity. And every colleague at Juelich forschungzentrum IBI-2, especially Dr. Gullermo Beltramo, George Dressdin, and Samar Tarazi, who made this work come true.

I would like to thank my family- my parents; Sahem, and Hasnaa, who raised me to chase my dreams no matter what it takes as they well be with me always and to my brothers; Maen and Rasheed, whose love and guidance are with me in whatever I pursue.

Declaration

I, the undersigned, declare that I submitted the thesis entitled:

DEVELOPMENT OF NON-COVALENTLY FUNCTIONALIZED MULTIWALLED CARBON NANOTUBES BASED-SUBSTRATE FOR SUPPORTING IN VITRO NEURONAL GROWTH

I declare that the work provided in this thesis, unless otherwise referenced, is the researcher's own work, and has not been submitted elsewhere for any other degree or qualification.

Student's Name: **Rama Sahem Hendawi**

Signature: 

Date: **22/06/2023**

List of Contents

List of Tables

List of Figures

List of Schemes

DEVELOPMENT OF NON-COVALENTLY FUNCTIONALIZED MULTIWALLED CARBON NANOTUBES BASED-SUBSTRATE FOR SUPPORTING IN VITRO NEURONAL GROWTH

By

Rama Sahem Hendawi

Supervisors

Dr. Naim Kittana

Dr. Mohyeddin Assali

Abstract

Background: Nerve injuries are considered the first leading cause of disabilities and one of the leading causes of deaths globally, which add a huge burden on socioeconomics. Many interventions have been developed to treat nerve injures, the golden standards are neurorrhaphy when suturing is possible, and autologous nerve transplantation, although promising results were obtained, functional recovery from chronic injuries remains a challenge. As a result, nerve tissue engineering emerged to find innovative solutions. In this study, the researcher aimed to develop neuronal growth by enhancing multiwall carbon nanotubes (MWCNT) dispersion and use it as a substrate.

Objectives: This study aimed to test the effect of CNT substrate on neuronal functions and morphology, by first enhancing the MWCNT dispersion and form a substrate allows neuronal growth.

Methods: in order to enhance MWCNT dispersion, the researcher functionalized it with poly-l-lysine (PLL) and chitosan by sonication, the cells were primary isolated from cortical rat embryo and seeded on PDMS polymer, and then we analyzed the substrate was analyzed by Raman spectra and scanning electronic microscope (SEM). Then we tested neuronal synchronicity was tested by calcium dye staining florescence, the recorded videos were further analyzed by SyincAnalysis software, the cellular viability, and synchronicity percentages were statistically analyzed by student T test. The neuronal morphology was analyzed by staining actin and tubulin, the main cytoskeletal filaments engaged in neuritogenesis, the recorded images were further analyzed by special software, and the results were statistically analyzed by one way ANOVA.

Results and conclusions: PLL enhanced MWCNT dispersion better than chitosan, with 0.05% PLL-MWCNT as our working concentration. For neuronal synchronicity the researcher tested the substrate against PLL-ECM as a control, and it was that there is found no significant difference between active cell number percentage and synchronicity cell percentage which indicates the substrate ability to sustain neuronal activity. Furthermore, we tested neurite branching against PLL and PLL-ECM as controls, and we found significant difference between PLL-MWCNT and others, we hypothesized this increase due to nanoscale topography that are in the favorable size for focal adhesion attachment, and that PLL-MWCNT increased substrate stiffness.

Keywords: Carbon nanotubes; poly-l-lysine; chitosan; synchronization; neuritogensis; nerve tissue engineering; substrate.

Chapter One

Introduction

Neurological disorders are one of the most serious health problems worldwide, it is one of the leading causes of death sharing 16.5% of deaths globally, and the first leading cause of disabilities (1), which add a huge burden on socioeconomics, especially that neurological disorders are linked proportionally with the population growing and aging (2), resulting in a substantial increase of patients in need for neuronal implants to improve the regeneration of damaged tissues.

Neurological injuries are a formidable challenge due to the complexity and the wide range of functions of the nervous system, it is the main regulatory (3), communicating, and controlling system of the body, responsible for all mental activities including memory, thought, and learning (4).

1.1 Neuron overview

The nervous system communicates through nerve cells known as neurons. A neuron is composed of a cell body (soma) that receives information through membranous projections called dendrites, transmitting it along cytoplasmic extensions called axons (5). This transmission happens due to changes in the cationic gradient of sodium and potassium ions across the plasma membrane, producing a propagating electrical impulse called action potential (6) which at the end of axons (nerve terminals) induces the release of neurotransmitters in the synapses formed between the axonal growth cones of the proximal neuron and the dendrite branching of the distal neurons (5). (Scheme 1).

Scheme 1

Nerve cell anatomy Graphic illustration of nerve cell anatomy showing the cell body (soma), the axon, and the direction of the action potential, it also shows the synaptic cleft and neurotransmitter vesicles release

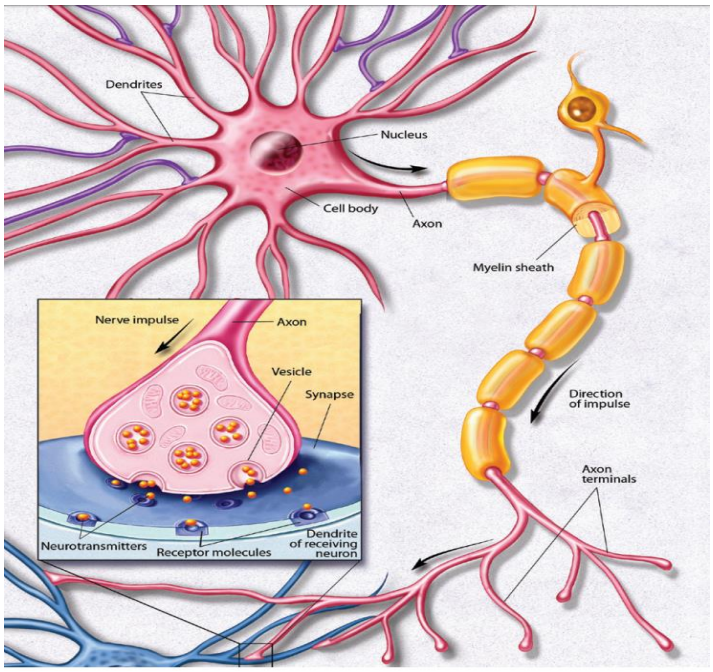

Note. The image was adopted from Navidmoghaddam A et. al., Year. 2014 (7).

Brain complex circuitry and functional synapses connection are formed by Neuritogenisis (Scheme 2). It is the process of extending axons and dendrites (8), mainly due to the accumulation of cytoskeletal actin and microtubules (9). It occurs in three stages, starting with the protrusion phase where the F-actin filaments rearrange and polymerize in discrete regions pushing these leading edges of the membrane forward to form lamellipodium and finger-like filopodia forming growth cones, -which the cell will use to detect the extracellular cues (10, 11), in the engorgement phase the microtubules follow these edges with transport organelles and vehicles to the periphery. Finally, the consolidation phase, where the microtubules become more bundled and actin filament more aligned which in turn gives the neurite a cylindrical shape (12).

At this stage, dendrites start arborization to form a fine meshwork of spines and synapsis, which will receive the input information to the neuronal cell body (13), and one of the formed neuritides has the potential to be the axon according to the extracellular signals that direct and guide axon growth cones to its final destination (12). The axon transmits the propagating action potential to its terminals by voltage-gated

sodium channels, inducing Calcium uptake through voltage-dependent calcium channels, which in turn triggers the release of neurotransmitter-filled vesicles to the synaptic cleft (14).

Axon path guidance, dendrite branching and elongation, and synaptic plasticity are the result of the interaction of the neuronal cell with the adjacent cells' proteins or the extracellular matrix (ECM) microenvironment molecules such as laminin, collagen, fibronectin...etc., through cell adhesion molecules (CAMs) (15). Cell-ECM interaction is regulated by the heterodimeric transmembrane receptors family called integrin, found in the point contacts on the filopodia. When integrin binds to external molecules, they become activated and dimerize, this in turn will recruit proteins like vinculin and talin to the cytoplasmic domain, thereby connecting the cytoskeletal actin to the ECM (16).

Scheme 2

Lamellipodium and filopodium formation during neuritogenesis and the activation of integrins

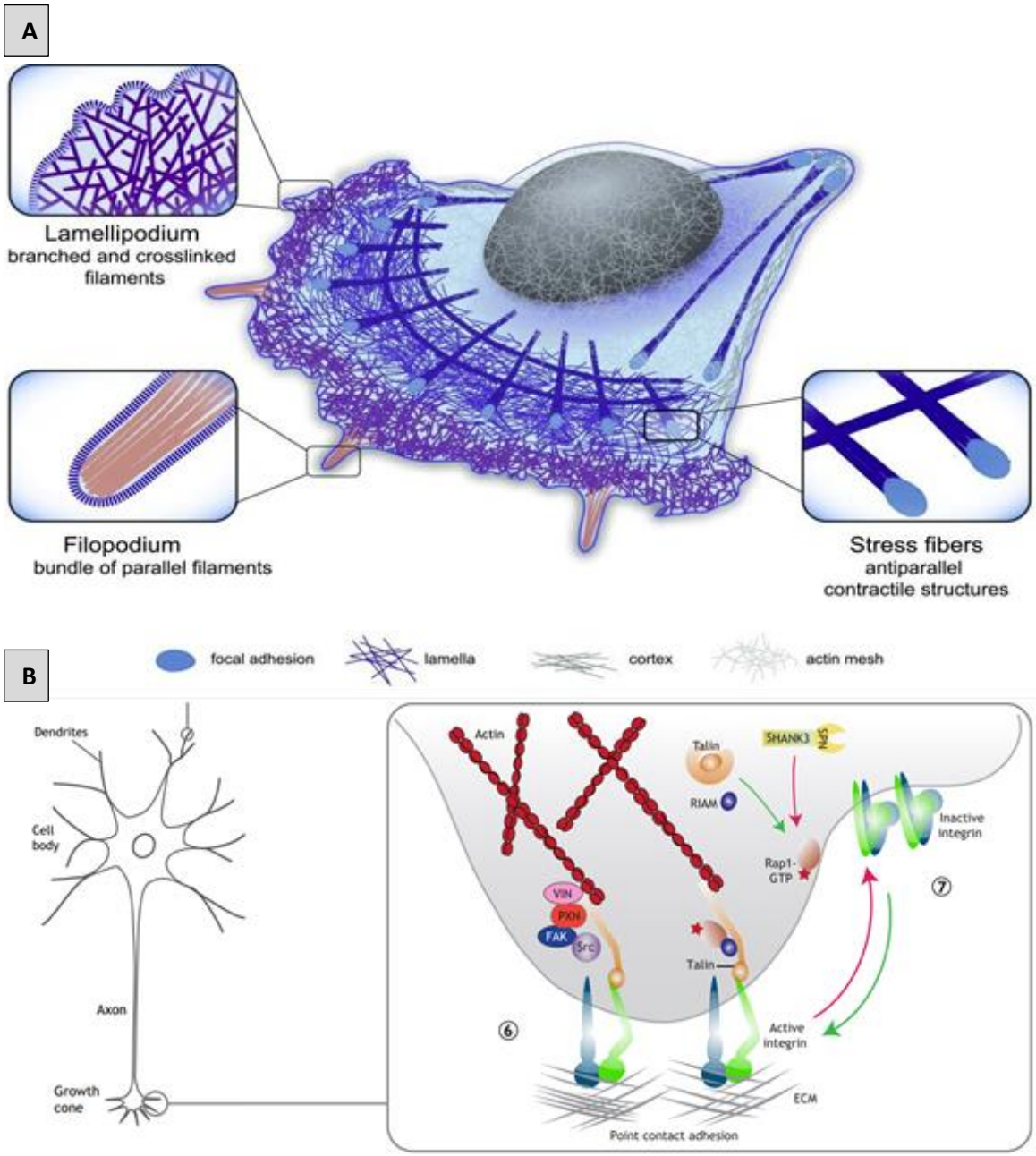

Note. A: Schematic representation of actin structures during neuritogenesis, lamellipodium is formed during the protrusion phase as dense crosslinked filaments, once formed filopodium emerges as a finger-like structure with bundles of parallel filaments, and lastly the stress fibers the dynamic structure which plays a significant role in the mechanical response.. B: Representation shows the activation of integrin after binding to ECM and its interaction with intracellular proteins to connect actin filament A**:**The image was adopted from Letort G et. al., 2015(17). B: The image was adopted from Lilja J et. al., 2018 (16).

Other adhesion receptors play a role in directing cells to form synapses, the major receptors in cell-cell interaction are the cadherins family, they are calcium-dependent hemophilic transmembrane proteins that consist of five extracellular cadherin repeat, they are connected to the cytoskeletal actin through cytoplasmic partner called catenins, cadherin-catenin complex regulates actin polymerization (18). Nectin is another cell-cell hetero-homo-trans-membrane adhesion receptor and it is connected to actin filament through afadin, an actin filament binding protein, it is connected through nectin-1 localized on the presynaptic axon terminals to nectin-3 on the postsynaptic dendrite spines (19).

1.2 Pathophysiology of neuronal damage

The human nervous system is divided into the peripheral nervous system (PNS) and the central nervous system (CNS). Understanding the molecular mechanisms of neurological injuries is considered to be the first step towards an effective treatment (20).

The peripheral nervous system (PNS) simply consists of motor and sensory neurons that receive and transmit information from body organs towards the central nervous system (CNS) and vs versa by the axons connected to the body somas in the spinal cord, each axon is surrounded by a connective tissue layer called endoneurium, and axons are grouped as bundles called fascicles and the latter are separated from each other by perineurium and another internal epineurium layer, all fascicles groups are wrapped together by an outer epineurium layer to define the nerve structure (21) as illustrated in Scheme (3A).

Peripheral impairment can range from mild discomfort to paralysis, depending on the degree of damage. Starting from Neurapraxia the mildest case which occurs due to compression leading to demyelination without further damage to the connective tissues layer of axons, resulting in slower conductive velocity, which promotes muscle weakness. The next level which involves axon damage in addition to demyelination is called axonotmesis and it is ranging from grade II to grade V neurotmesis as stated by Seddon and Sunderland classifications of nerve injuries (22).

After organ denervation the recovery from peripheral nerve injury mainly has two options according to the percentage of damaged axons within a nerve, when less than 30% are injured, the dominant recovery mechanism would be collateral sprouting of new axons, it can take from 4 days to 6 months for recovery, however, with more time it takes, the denervated muscle will be subjected for atrophy, on the other hand, sprouted axons which don't receive neurotrophic factors from the end organ will eventually degenerate. Injuries involving more than 90% of axons damaged, they largely rely on three processes: Wallerian degeneration, axon regeneration, and target organ innervation. Within the first week, the cellular and molecular events of the Wallerian degeneration process switch on upon the breaking of the axon's cell membrane or myelin leading to swelling at both ends of injury (23), the sudden inflow of ions such as Na^+ and Ca^+ will initiate a cascade of cellular events serves to recruit and induce the migration of phagocytes and macrophages to the injury site under the effect of Schwan cells signals like monocyte chemoattractant protein-1 (MCP-1) as well (24), to remove the debris and myelin residues, during macrophage clearness they release recruiting factors for Schwan cells so later they will differentiate and proliferate on the remaining endoneurial tube forming what is known as bands of Bungner (25). When the Wallerian process is finalized, axonal regeneration takes place starting from the tip of the proximal injury site, the axon will be able to regrow and sprout growth cones under the influence of calcium, as long as it is still intact to the cell body, while the distal part (after the injury site) will degenerate keeping the formed bands of Bungner channel to guide the growth cone's filopodia towards the targeted organ (26), Schwann cells forming bands of Bungner have a substantial role on regeneration, as they promote gene expression of regeneration by interacting with tyrosin kinase receptors, furthermore, it is an essential reservoir neurotrophic factors in addition they produce neurite-promoting factors, which engage with ECM such laminin and fibronectin, promoting growth cones adhesion alongside the endoneurial tube. It will take up to 4 months for the bands of Bungner to be filled before it shrinks (25). The recovery process is completed by a maturation process where newly formed axons enlarge and re-myelinate for functional recovery (27). on the other hand, Studies have shown that periphery nerves are not able to restore their function when the neural defect is more than 5mm in length (28).

Scheme 3

Schematic illustration of Peripheral nerve anatomy and the axon regeneration process

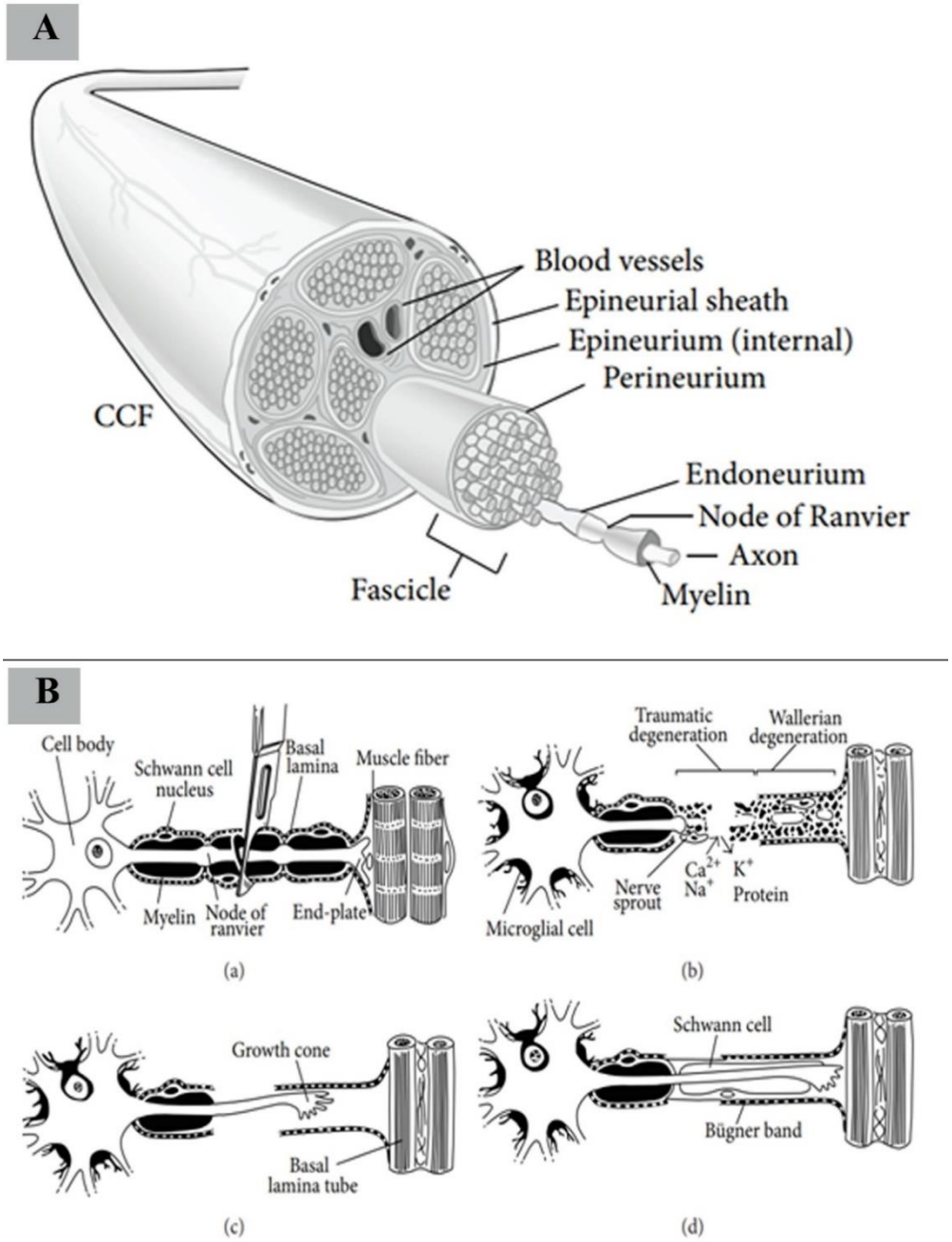

Note. A: Peripheral nerve anatomy. B: Axon regeneration process (Ba) Represent a full axon injury. (Bb) Show the Wallerian degeneration process. (Bc) The nerve sprouting of growth cones and its direction toward the target organ. (Bd) The maturation process and the functional recovery restoration. A and B images were adopted from Grinsell D et. al., 2014 (21).

On the contrary, the CNS does not have the same ability for regeneration as the PNS, it is regenerative capacity is limited by the inhibitory effect of glial cells (astrocytes and microglia) after they are recruited to the injury site and by the slower degeneration of the distal segment of the axon which results in the accumulation of myelin debris. Both factors form what is known as a glial scar (29). This inhibitory environment does not only affect the axonal regrowth but also neurite repair and the differentiation of neurons.

1.3 Current approaches to neuro-regenerative applications

Many interventions have been developed to induce neurological injury recovery, but only a few have succeeded. The current first option is neurorrhaphy when the neuronal injury gap is small in length and end-to-end suturing is possible, it is a surgical technique that relies on suturing neuronal gap with suitable correct orientation following fascicles alignment, most common suturing techniques are: Epineurial suturing, Fascicular suturing, and Epi-perineurial suturing, but neurorrhaphy has a lot of restrictions, for example, it is not effective when the neuronal gap is large, and it might generate foreign body reactions by the suturing materials which may lead to scars (30).

When the defect length is more than 5mm, and the suturing becomes impossible, then allogeneic and autologous transplantation become the main treatments for PNS injuries (2), as they involve filling and bridging the gap with graft either by a self-donated or external matching donor, but they are subjected to many disadvantages, including limited donor sites, the need for multi-surgeries, and the mismatch between the donor nerve and the damaged one (31). Although promising results were obtained, functional recovery from chronic injuries remains a challenge (32), even for CNS injuries there is no current effective treatment to restore nerve functions due to the inhibitory environment that restricts neuronal regrowth. Therefore, such patients rely on lengthy rehabilitation therapy, which is based on training the remaining nerves to compensate for the function of the injured neurons (33). All these obstacles have pushed forward developing new interventions aim to enhance functional recovery with the least collateral damage possible.

1.4 Nerve tissue engineering

Neural tissue engineering is an emerging field to support PNS and CNS injuries, it is based on designing biomaterial constructs and implants which artificially re-create extracellular cues to support and direct neuronal growth and restore neuronal communication and functional circuitry (34), especially, since the external environment physical topography, biochemical and electrical cues have a great influence on the growing neuron (35), as a replacement of neuronal grafts.

The ideal scaffold material should possess certain characteristics to be able to mimic the natural extracellular matrix (ECM). First, it has to be biocompatible, allow cell adhesion and proliferation, and sustain suitable functionality of cells on the fabricated scaffolds (34). Second, biodegradability, the scaffold is preferred to biodegrade by the tissue enzymes to limit the surgical intervention, and to decrease the risk of inflammation. Third, the scaffold should offer multiple cues such as mechanical, topographical, biochemical, and electrical properties to mimic the natural extracellular environment for convenient neuronal behavior (28). There are different kinds of scaffolds each has pros and cons.

Natural polymers are either purified proteins and or crude mixtures of ECM molecules including (collagen, gelatin, hyaluronic acid, and chitosan). Natural polymers are the most commonly used until now, due to their remarkable advantages, such as biodegradability, facilitated cell adhesion, and cell-biomaterial interaction, and minimal ability to induce inflammatory responses. However, their poor mechanical properties, and the inadequate degradation time, limited their use in injuries that require a longer duration of support (36, 37).

Synthetic polymers, such as silicone, poly ε-caprolactone (PCL), and poly L-lactic acid (PLLA), were developed to overcome some of the natural polymers' shortcomings. These polymers were fabricated with enhanced mechanical properties and it is even to optimize their composition to obtain a slow degradation profile. Furthermore, the manufacturing process would allow the casting of aligned polymer fibers which will offer some sort of direction cues for neuronal regrowth (37).

FDA has approved some fabricated biocompatible and biodegradable conduits, but their use is limited as they do not satisfy the ideal scaffold characteristics, and their coverage is not convenient for neural damage of longer than 4cm (38). Nano-based materials opened a new door for developing an ideal scaffold especially carbon nanotubes for their unique and interesting characteristics.

1.5 Carbon nanotubes overview

In recent years, among synthetic materials carbon nanotube-based scaffolds have grabbed the attention for potential use in neuro-regeneration applications, as a novel tool able to tune nerve cell behavior after its discovery in 1991 by Sumio Iijima (39).

Carbon nanotubes (CNTs) are cylindrical nanostructures of rolled graphene sheets with a diameter in the nanoscale range (0.4-100 nm) and lengths up to micrometers. They are classified according to graphene layers composition into single-wall carbon nanotubes (SWCNTs), and multiwall carbon nanotubes (MWCNTs) (40) as shown in scheme (4A).

Carbon nanotubes applications seem to be limitless for their remarkable properties, the sp^2 hybridization between carbon atoms acquired them high tensile strength that can be hundreds of times higher than steel, CNTs also shows high young's modulus for their elasticity, and they are also good thermal and electrical conductors.

However, due to the van der Waals forces and π–π electron interactions between CNTs cylinders, they tend to agglomerate in relatively large masses which decreases their dispersion in biological fluids prevent making use of their nanometric properties, and increases their cytotoxicity (41), which in turn limit their use, so enhancing CNTs dispersion is considered the first crucial step to access CNTs advantages.

Enhancing carbon nanotube dispersion in biological media can be done through different techniques, either physically, by applying external mechanical forces such as shear mixing and ultra-sonication (42), or by chemical functionalization covalently or non-covalently as in scheme (4B). Covalent functionalization may form more stable functional group attachment by incorporating reactive groups such as carboxyl or amino groups, but it introduces side wall defects (43) and might change carbon nanotube characteristics due to shifting the hybridization from sp^2 to sp^3. Non-covalent

functionalization is based on Vander Waals interaction by incorporating hydrophilic substances such as surfactants, polymers, and aromatic substances, it can extend beyond that to bio-functionalization, using biological factors not only enhance the CNTs dispersion but also afford cellular activity (44). However, this functionalization is sensitive and susceptible to thermal and pH changes.

Scheme 4

CNTs cylindrical structure and CNTs functionalization techniques

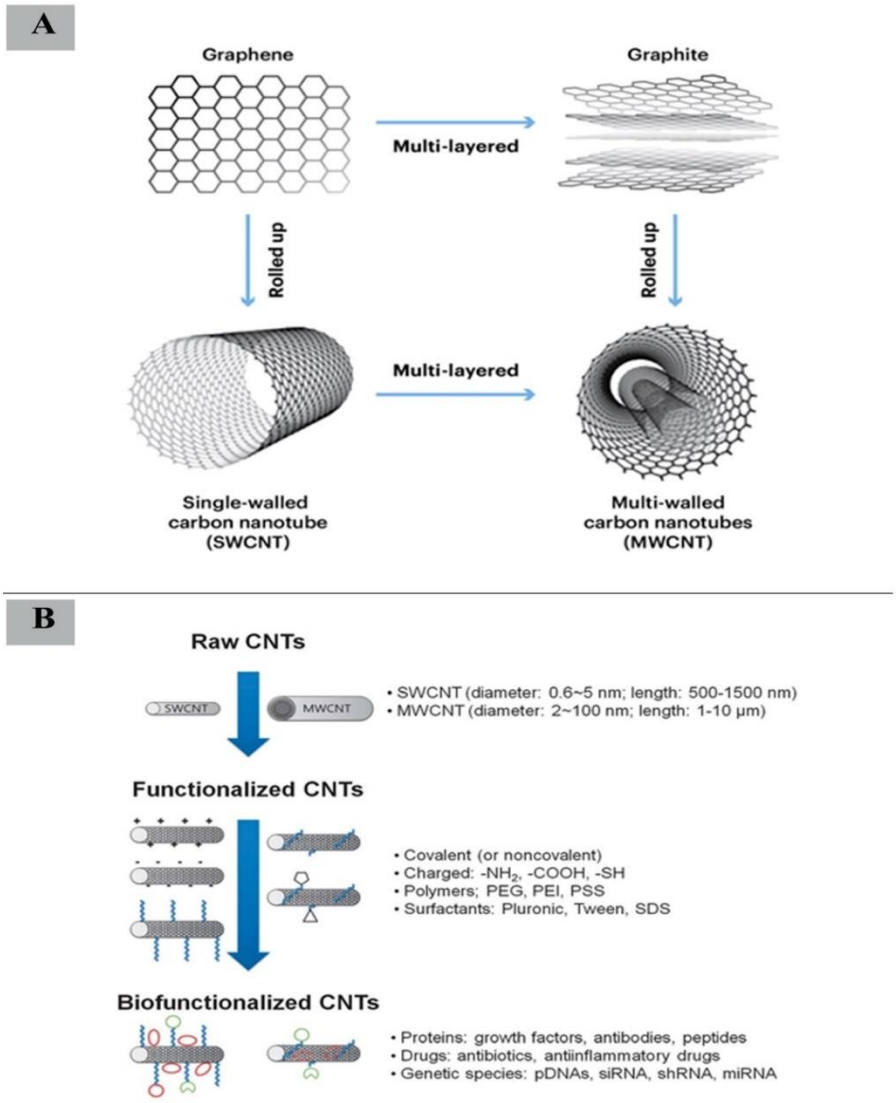

Note. A: Schematic illustration of carbon nanotubes' cylindrical structure as single-wall and multiwall carbon nanotubes. B: Scheme of carbon nanotubes with different functionalization techniques. A: The image was adopted from Marrina Flichakova et. al., 2021(45). B: The image was adopted from Hwang J-Y et. al., 2013 (44).

1.6 Carbon nanotubes utilization in nerve tissue engineering

This material is becoming a leading edge of nanotechnology approaches in neuro-medicine, for its well-documented thermal, mechanical, and electrical properties (46). Furthermore, its nanostructured topography may constitute promising extracellular cues to direct and enhance neuronal elongation and branching, as its cylindrical shape is reminiscent of neuronal distal dendrites (47) and familiar to extracellular matrix fibers.

In addition, it is found that neuronal focal adhesions attach more preferably to molecules in the range of [5-200]nm (48) as it resembles natural extracellular matrix proteins' nanoscale dimensions. On the other hand, CNTs are electrically conductive materials, which may support electrically propagating tissues such as neurons, finally, their low biodegradability profile makes them perfect material as implantable devices where long-lasting support is required (48, 49).

There are two main strategies for using functionalized carbon nanotubes in neuroregenerative applications: first the direct addition method, the CNTs are directly added to cell culture media, in this method CNTs are allowed to interact and penetrate through the cell, as a part of the nano-delivery system, or second, it can be through designing a substrate for cellular growth support in the scope of implantable devices development (44).

Scheme 5

CNTs strategies in neuroregenerative medicine

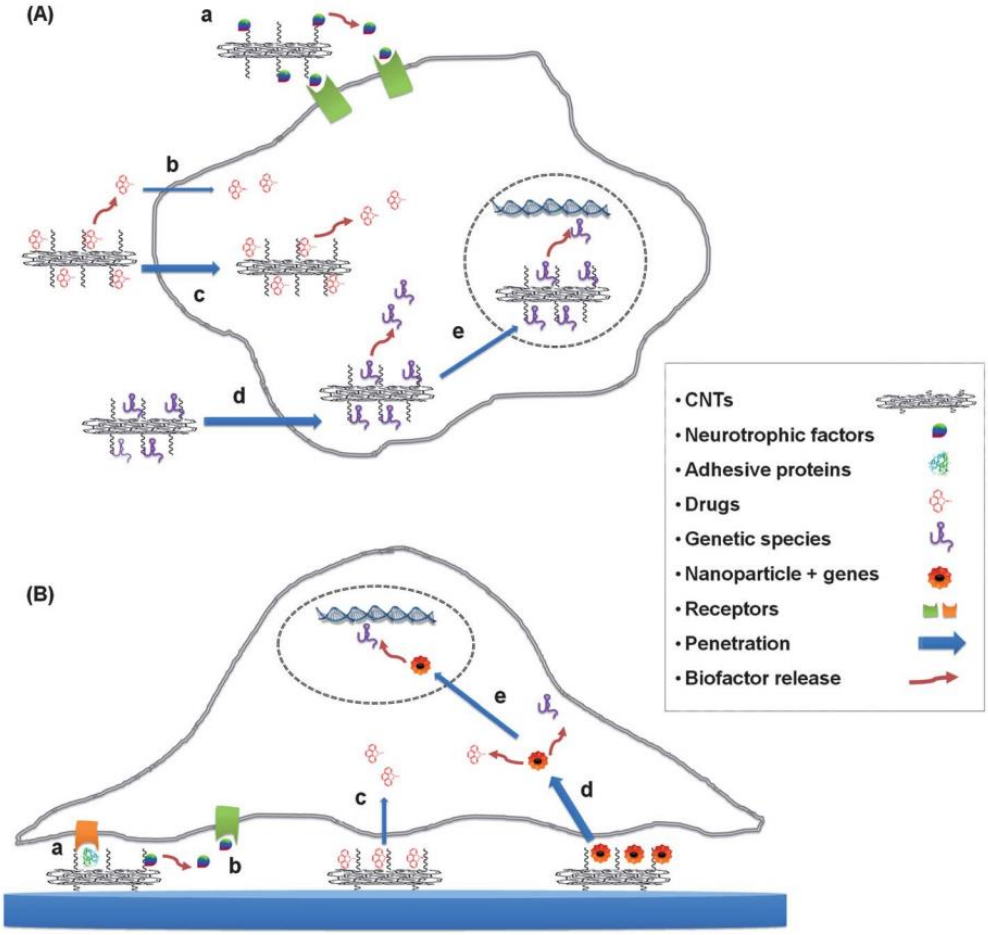

Note. Drawing showing the possible strategies to use CNTs in neuroregenerative medicine. (A) Represents the nano-delivery system in the direct addition method. (B) Represents using CNTs as a substrate. The image was adopted from Hwang J-Y et. al., 2013 (44).

The first demonstration of using CNTs as a substrate for neurons was provided by Matteson *et. al*, they investigated the influence of CNT modification on neurite growth, they cultured hippocampal neurons on CNTs coated with 4-hydroxynonenal (4-HNE) a lipid peroxidation product, their scanning electron microscope (SEM) examination suggested increased in neurite number formation compared to the control unmodified CNTs surface (50), later Hu *et. Al* (51) have investigated the relation between CNTs functionalization electrical charge and neurite growth, they have used MWCNTs functionalized with a negatively charged carboxyl group, neutral poly-m-aminobenzene sulfonic acid (PABS) as zwitterionic, and positively charged ethylenediamine (EN), they observed a significant increase in the average neurite length and neurite

arborization in neurons growing on positively charged MWCNTs compared to neutral and negative charge respectively.

Scheme 6

MWCNTs electrical modulation effect on neurite branching Schematic drawing illustrating the effect of MWCNTs electrical modulation on neurite length and branching. Which shows an increase in neurite branching with positive charge MWCNTs

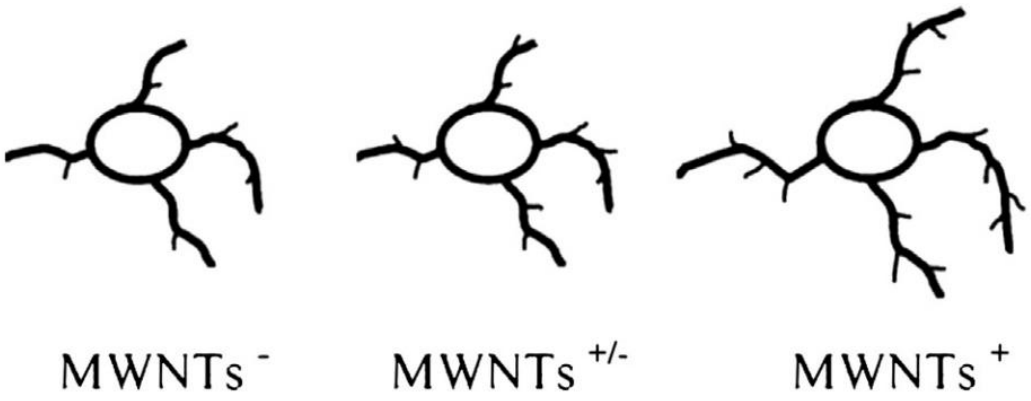

Note. The image was adopted from Hu H et. al., 2004 (51).

This pivotal study established for the first time, that neurite branching and formation can be modulated by CNTs chemical alterations, which pave the way for CNTs optimizations toward designing an effective system in neuro-regenerative medicine (48). The remarkable CNTs topographical features are not limited to influencing neuritogenesis but also it could control neurons growth direction and elongation, the first evidence was revealed in 2005 by Zhang and colleagues, who cultured hippocampal neurons on geometrically patterned MWCNTs arrays, and they observed that neurite growth followed the patterned MWCNTs (52), interestingly, later studies who investigated the same concept found that neurites growing under the direction of CNT pattern tend to extend further and faster compared to self-directed neurites (53). In addition to topographical influence and surface charge, electrical conductivity is one of the distinguished features of CNT, this was tested by Malarkey and colleagues, who grew hippocampal neurons on a glass substrate sprayed with different layers of CNT solution functionalized with polyethylene glycol (PEG), the different thickness produced different conductivity as follows (0.3, 28 and 42 S/cm), the difference in films conductivity didn't mainly impact neurite branch number, but the film with the least conductivity (0.3 S/cm) significantly increased the average neurite length, this study

highlighted the importance of controlling CNT films thickness and conductivity, as CNT films are able to boost neurite length through a narrow range of conductivity (54).

Many research groups worldwide are devoted to optimizing the functionalization of CNT to allow their utilization in neuronal network regeneration, but there is still a scientific gap for more development, as some of them try to enhance CNT dispersion by using strong acids to introduce carboxyl groups on the side wall offering moieties for covalent functionalization. However, it was found that this method results in major defects on the side walls of CNT which would, in turn, affect some of its characteristics most likely decreasing Young's modulus (55). Finding an efficient functionalization of CNTs that would enhance their dispersion to form an ideal substrate for better neuronal growth is a looking forward.

In our project, we used natural polymers; Chitosan and Poly-L-lysine (PLL), to non-covalently functionalize CNTs, to avoid any defects in the CNT wall.

Chitosan (CS) is a polysaccharide formed by the deacetylation of chitin, found in the exoskeletons of arthropods. Chitosan is one of the most intriguing natural biomaterials used in tissue engineering, especially nerve tissue engineering, for its remarkable properties, it is a biodegradable and biocompatible material with nontoxic metabolite and antimicrobial activity (56, 57). Many studies have shown the ability of chitosan films to enhance neuronal outgrowth, as a result, chitosan tubes became FDA-approved in 2015 for peripheral nerve repair < 1 cm long (58). Nevertheless, chitosan has debilitated mechanical stability, which might affect its application where a long-lasting implant is required (59). Carbon nanotube/chitosan functionalization would form a balanced material where chitosan is hoped to improve CNT dispersion and CNT would improve the mechanical properties of chitosan.

Poly-L-lysine (PLL) is a hydrophilic cationic biopolymer that consists of alpha-lysine as a monomeric unit, which is one of naturally 20 essential amino acids that play a vital role in injury recovery and as a protein building block, on the other hand, it is commonly used to coat hydrophobic solid surfaces like glass slides to make them suitable for cell adhesion, spreading and differentiation, especially in serum-free media, as PLL contains positively charged positions that function as attachment spots for negatively charged membranous proteins of cells (60), Therefore, combining PLL with

CNTs might enhance cellular adhesion and, at the same time, provide polar moieties to the CNTs that enhance their dispersion.

In this project, we hypothesized that a properly functionalized CNT substrate may enhance neuronal circuit synchronicity between cells and increase neuron branching of the single cell.

1.7 Aims and objectives

1.7.1 General aim

Our project aims to test the effect of MWCNTs substrate on neuronal functions and morphology.

1.7.2 Specific objectives

- Employ chitosan or PLL to enhance the dispersion of the pristine form of MWCNTs in hydrophilic media.
- Seed the cells on top of the surface and grow them for several days.
- Evaluate cellular functionality and morphological changes.

1.7.3 Significance of the study

As mentioned above, the neuronal injury field is still lacking an efficient treatment or ideal implant to direct neuronal growth and restoration of the functionality of damaged neurons. This study is expecting to find an efficient, easy, cost-effective way to design a 2D model substrate that would increase neurite branching and enhance neuronal circuit communication, by using the advantages of MWCNTs as a part of basic research for designing a future implant that is biocompatible, offer a controlled biodegradability profile, lined inside with carbon nanotube layer which can take the lead in directing neurons re-growth process.

Chapter Two

Materials and Methods

2.1 Materials

2.1.1 Consumables and chemicals

Table 1

Lab consumables

Lab consumables	Company
Petri dish 3.5 cm with predrilled 2.5 cm holes	Cell E&G , San Diego, USA
Cover slip ø 12 mm #1; 25 mm #0	Menzel, Braunschweig, Germany
Microscope slides, plain	Brand, Werlheim, Germany
Parafilm	VWR, Darmstadt, Germany
Plastic spatula	Brand, Werlheim, Germany
Reaction tube 1.5 mL, 2 mL	Eppendorf, Wesseling/Berzdorf,Germany
Reaction tube 15 mL, 50 mL	Greiner Bio-one, Frickenhausen,Germany
Cell culture dish 35 x 10 mm	Greiner Bio-one, Frickenhausen, Germany

Table 2

Chemical materials

Chemical	Company
B-27 Supplement	Thermo Fisher Scientific, Massachusetts, USA
Chitosan medium molecular weight	Sigma, Taufkirchen, Germany
Formaldehyde 37%	Merck, Darmstadt, Germany
Gentamicin (50 mg/mL)	Sigma, Taufkirchen, Germany
GlutaMAX Supplement (100X)	Thermo Fisher Scientific, Waltham, USA
Glycine	Sigma, Taufkirchen, Germany
Hank's Balanced Salt Solution (HBSS)	Thermo Fisher Scientific, Waltham, USA
4-(2-hydroxyethyl)-1 piperazineethanesulfonic acid (HEPES)	Sigma, Taufkirchen, Germany
Hibernate-E Medium	Thermo Fisher Scientific, Waltham, USA
Multiwall carbon nanotube	Riverside, CA, USA
Magnesium chloride (MgCl2)	Sigma, Taufkirchen, Germany
MES (2(N-Morpholino)-ethanesulfonic acid)	Sigma, Taufkirchen, Germany
Neurobasal Medium (1X)	Thermo Fisher Scientific, Waltham, USA
Milk powder	Roth, Karlsruhe, Germany
Phosphate-Buffered Saline (PBS) pH 7.2	Thermo Fisher Scientific, Waltham, USA
Poly-L-lysine solution Mol wt 150,000-300,000; 0.01%	Sigma, Taufkirchen, Germany
Sodium chloride	Sigma, Taufkirchen, Germany
Sylgard® 184 silicone elastomer kit (PDMS)	Dow Corning, Wiesbaden, Germany
Triton-X-100	Sigma, Taufkirchen, Germany
Trypsin-EDTA, 0.05% trypsin 0.2% EDTA	Sigma, Taufkirchen, Germany

2.1.2 Devices

Table 3

Experimental devices, imaging systems, and software used

Lab instruments	Company
Clean bench HeraSafe	Heraeus, Osterode, Germany
CO2 - Incubator Typ B12	Heraeus, Osterode, Germany
Delta 10 TT spin coater	Suss-Micro Tec, Garching, Germany
Desiccator	Duran Group GmbH, Wertheim/Main, Germany
Vortex mixer	VWR, Radnor, USA
Water bath WNB-22	Memmert, Schwabach, Germany
Microscope Axiovert Imager-M2	Carl Zeiss, Jena, Germany
Microscope Axiovert 40 CFL	Carl Zeiss, Jena, Germany
Axio observer	Carl Zeiss, Jena, Germany
Axio imager Z2 upright	Carl Zeiss, Jena, Germany
Plan-Apochromat Ph2 20x air (NA 0.8)	Carl Zeiss
Plan-Apochromat 10x air (NA 0.45)	Carl Zeiss
Plan-Neofluar Ph3 63x oil (NA 1.25)	Carl Zeiss
Image J	Wayne Rasband, U.S. National Institutes of Health, Bethesda, USA
Zen blue 2012	Carl Zeiss, Jena, Germany
Graph Pad Prism	GraphPad Software, San Diego, USA
Solis	
BranchAnalysis	Juelich FZJ, Germany
SyincAnalysis	Juelich FZJ, Germany

2.1.3 Media and buffers

Table 4

Media, buffers, and coatings used in cell experiments

Media/buffer	Components	Concentration
Neurobasal Media	Neurobasal medium	97%
	B-27 Supplements	2%
	GlutaMAX Supplement (100 X)	1%
	Gentamicin	1 µg/ml
Cytoskeletal Buffer (1X CB), pH:6.1	EGTA	5 mM
	Glucose	5mM
	MES (2(N-Morpholino)-Ethansulfonacid)	1.95 g/L
	MgCl2	10 mM
	NaCl	150 mM
	Streptomycin	1.72 mM
HEPES Buffer, pH: 7.2	HBSS	200 ml
	HEPES	0.02 M
	Pluronic acid	0.04%
Epatch Media, pH 7.2	NaCl	120 mM
	KCl	3 mM
	$MgCl_2$	1 mM
	HEPES	10 mM
	$CaCl_2$	2 mM
PLL-ECM coating (10ml)	Cold PBS	9 ml
	PLL	1 ml
	ECM	125 µL
	Cold PBS	9ml

2.2 Methods

2.2.1 Substrate preparation

2.2.1.1 PDMS polymer fabrication

Polydimethylsiloxane (PDMS), is a silica-based polymer that is fabricated to design elastomers of controllable stiffness (61). PDMS-based polymers are widely used in cell culture applications for being biocompatible with cells, transparent so that it would allow observing cells growing in cell culture dishes via inverse and upright microscopes, and can be fabricated into molds with deformation ability and different stiffness profiles for mechanical applications. We chose to grow cells on PDMS polymer to fabricate a surface with a stiffness profile as close as possible to mimic the neuronal natural stiffness environment (62).

The PDMS surface was fabricated by first mixing the base polymer with its cross-linker (methylhydrosiloxane-dimethylsiloxane) in a 1:40 ratio (cross-linker: base polymer) - to yield a stiffness of 50 kPa. The components were mixed vigorously for 10 mins, then it was degassed in a desiccator to remove air bubbles so they would not affect surface transparency.

About 300 µL of PDMS were added to a round glass slip (#0, Ø 25 mm, Menzel) to coat its surface by a spin coater, at 1800 rpm for 15 sec to have 90-100 µm PDMS thickness. Cell culture dishes were prepared by using a 3.5 cm- Petri dish, which bottom is predrilled with a 2.5 cm hole. The drilled petri dish was placed on the coated glass and was put in the oven at 60 °C for 16 hrs to allow crosslinking. By these parameters, we had constant thickness for all experimental dishes and appropriate thickness for inverse microscope visualization.

2.2.1.2 Functionalization of MWCNTs

First MWCNT powder was sterilized by exposing it to UV light for 15 mins, with stirring the powder every 5 mins. To coat MWCNTs with chitosan, we prepared 0.1% w/v chitosan solution in 1% v/v acetic acid solvent and sterilize it with a syringe filter. After that, we added 0.01 g of MWCNT to 1 ml of chitosan solution, but we found in later experiments that the chitosan-MWCNTs complex formed a layer that detached spontaneously from the PDMS surface after it was dried, in addition, the surface was

rough and thick so that it obscured the microscopic observation of the cultured cells on its surface. For these reasons, we abandoned coating MWCNTs with chitosan and decided to proceed with PLL functionalization.

For PLL functionalization, we mixed 0.01 g MWCNT with 1 ml 0.01% w/v commercial-ready use PLL. For control, we added 0.025 g of MWCNT in 2.5 ml of distilled water. All mixtures were sonicated for 1 hr on the maximum power of the sonicator at 22°C temperature. To test PLL-MWCNT dispersion stability we centrifuged 2 ml of the suspension at 4500 RPM for 30 mins.

2.2.1.3 Preparation of the substrate model

To prepare the experimental substrate films on the spin-coated dishes, we used the drop cast method, by adding a drop of the suspension on the dish surface and letting the water evaporate, but we found that the surface area of the predrilled dish requires a large volume to cover the whole area, so we optimized the system to save the stock material from deprivation and to increase the cell isolates used in the same experimental dish by using a commercial PDMS foil that has four holes and was placed on top of the PDMS surface as shown in figure 1.

Figure 1

Cell culture dish design for neuronal growth The final design used in the project, PDMS spin-coated dish with four holes PDMS foil on top where the PLL-MWCNT was drop casted

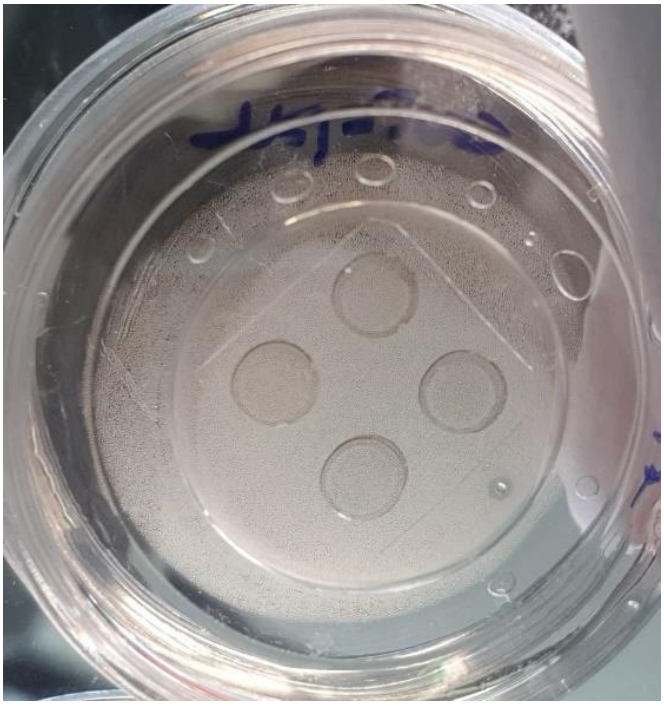

Under the hood, we added 20 µL from each mixture on each hole and were evaporated overnight at room temperature; after they were completely dried they were washed 3 times with distilled water.

2.2.2 Neurons experiments

2.2.2.1 Primary cortical neurons isolation

Pregnant rats (Wistar, Charles River, Sulzfeld) at 18-19 days of gestation were anesthetized by CO_2 before decapitation, then the embryo chain was removed, the embryos were sacrificed by cervical dislocation, the heads were placed in Hanks Balanced Salt Solution (HBSS) on an ice bath, then each head was transferred to a culture dish containing 2 ml HBSS under the hood. Under a dissecting microscope, the head was fixed with tweezers in the mandible area, the cranium was opened with other tweezers. The brain was taken out and the hemispheres were opened and spread, while the skin, stratum, and hippocampus were eliminated. After that, the outer parts were cut where the cortex is found, and the process of cell isolation would start immediately,

extra cortexes were stored in hibernated media at 4°C and can be used for up to 3 days, each replicate of the later experiments required new isolation.

The cortexes were put in 2 ml of cold trypsin for tissue digestion (0.05%) EDTA – as maximum of 4 cortexes per dish, and were incubated at 37°C for 15mins, with swirling every 5 mins, the tissues were transferred into 2 ml tube prefilled with 1 ml neurobasal (NB) media. The supernatant was removed and another 1 ml NB media was added, repeating this process three times in raw to clean the tissue from trypsin. In the last cycle, the tissue was triturated with 1 ml 30-40 times to dissociate the tissue and free the cells. We let the tube stand for 2 mins so the remaining tissue can settle down and separate from the cells in the supernatant, then the supernatant was removed to a new tube and centrifuged at 1000 rpm for 4.5 mins at 20°C, the supernatant was removed and the cells were re-suspended in fresh 1 ml NB medium.

The viable cells were counted using trypan blue, for synchronization evaluation we seeded cells at a concentration of 5×10^5 cells/dish and for morphological evaluation, at a concentration of 2×10^4 cells/dish, the required number of cells according to each experiment was suspended in NB medium to reach 500 µL for each experimental dish (63).

2.2.2.2 Coatings preparation

500 µL of PLL was added as a coating layer on PLL-MWCNT, PLL-ECM, and PLL dishes, and incubated overnight at room temperature, for PLL-ECM dishes 500 µL of PLL-ECM was added overnight as well before cell seeding PLL-ECM dishes were washed two times and the others were washed three times to remove excess coatings which could be toxic for cells. The media was changed every two days.

2.2.2.3 Neurons adhesion and viability

To determine the best working concentration, we tested the effect of three different PLL-MWCNT film thicknesses on neuronal adhesion and viability. We added 20 µL of PLL-MWCNT from the following concentrations (0.02, 0.01, and 0.005) % w/v on each hole on the substrate according to the previous method, we seeded 5×10^5 cells/dish, and we examined the cells on day 6; just to allow cells to grow and branch to detect

them by staining tubulin filaments, using immunocytochemistry protocol. The dishes were observed by an upright microscope using a 20x objective.

2.2.2.4 Measuring neurons synchronism

To detect the influence of the substrate on neuronal functionality and synchronism formation between neurons we used calcium imagining which relies on using an intracellular calcium dye Cal950, that once it penetrates the cell membrane the cytosol esterase cleaves its lipophilic blocking group, resulting in a negative charge fluorescence dye trapped inside, its fluorescence is enhanced when binding to calcium during the action potential process producing a signal when the cells are synchronizing (64).

We prepared the experimental dishes as mentioned before with 5 x 10^5 cells/dish, and on day 9 according to previous research from IBI-2, proved that neurons start synchronization at 9 and 5 x 10^5 cells/dish concentration. We started the calcium imaging. The medium was removed and the cells were incubated with Cal950 (0.5 M) for 2.5 hrs in HEPES buffer. Later, it was replaced with Epatch medium and incubated for another 10 mins before imaging.

An upright fluorescence microscope with a climate chamber adjusted to 37^{o}C was used for imaging. The samples were excited by a laser beam at 561nm. The imaging was done as short video clips of 3.3 mins duration. The imaging system was operated by Solis software with optimized parameters that are meant to reduce dye bleaching as follows:

Table 5

The final parameters used for all samples in calcium imagining by Solis software

Parameter label	Parameter type
Acquisition mode	Kinetic series
Exposure time	0.009987
Frame rate	15 FPS
Trigger mode	Internal
Kinetic series	3000
Image area	Full area
Pixel binning	4X4
Pixel readout rate	560MHz- fastest readout
Shuttering mode	Rolling
Sensitivity/Dynamic Range	16-bit (low noise and high well capacity)

This experiment was done in two rounds, in each round we prepared three replicates from PLL-MWCNT and the control PLL-ECM, each dish had four different cell isolates, and each hole was measured in two different positions.

2.2.2.5 Immunocytochemistry

To detect the effect of PLL-MWCNT substrate on branch formation we stained actin and tubulin filaments, the main cytoskeletal filaments engaged in neuritogenesis that are highly influenced by external topography cues.

The experimental dishes were prepared as mentioned before but using a diluted concentration to make sure that cells will precipitate as single cells, three dishes were prepared from each group; PLL-MWCNT, PLL-ECM, and PLL. After 48hrs the immunocytochemical procedure started, first we removed PDMS foils and fixed the cells by incubating them in 500µl 3.7% paraformaldehyde (PFA) in 1X cytoskeletal buffer (CB) for 15mins at 37°C, then the dishes were washed three times with Glycine-CB (30mM). After cell fixation we started cell staining by washing cells with 1X CB, incubating them with 500 µl of 0.05% TritonX-CB for 10 mins at room temperature, then we blocked the nonspecific binding sites with 5% milk powder-CB for 60 mins at room temperature (RT), Later, the cells were incubated with the primary antibody and phalloidin in 1% milk powder-CB overnight at 4°C.

The next day, the cells were washed three times with 1% milk powder-CB, then they were incubated with the secondary antibodies to attach to the primary antibodies and tag the fluorophore in 1% milk powder-CB for 80 mins, later they were washed three times with 1X CB followed by 1X wash with distilled water, lastly, 20 µl Gelmount was added after water removal in the middle of dishes, then we placed #1 coverslip on top without air bubbles. The antibodies and phalloidin were added according to the dilutions specified in table 6.

Table 6

Fluorescence staining reagents' dilutions

Filament	Primary antibody	Secondary antibody
Actin	No antibody	Phalloidin Atto (488) 1:500
Tubulin	Anti-Tubulin 1/L ½ Rat 1:500	Cyanine cy3 (591) Goat Anti-Rat 1:200

The stained cells were imaged by cell observer microscopy, using 63 X oil objective Carl Zeiss AG, Germany and Zen blue software. More than 500 cells were observed and analyzed from each group. The Cy3 fluorophore was excited with a laser at 561 nm and Phalloidin Atto at 488 wavelengths. The mean beam filter 488/543/633 was utilized to detect two fluorophores in one scan; all other parameters were kept constant for each scan (63).

2.2.2 Experiments analysis

2.2.3.1 Substrate analysis

2.2.3.1.1 Raman spectroscopy

Raman spectroscopy is one of the techniques used to determine the vibrational modes of molecules, which in turn can identify molecules by their structural fingerprint (65), we used Raman to test the existence of PLL-MWCNT on a spot on the surface, especially in the areas that look vacant under the inverse microscope, Confocal Raman microscopy was performed using an alpha300R setup (WITec, Germany). The sample was illuminated using a 532 nm excitation line from a single-mode frequency-doubled Nd: YAG laser via a 100 mm single-mode glass fiber. An LD EC Epiplan-Neofluar 50x/0.55 objective (Carl Zeiss AG, Germany) was used and the laser power at the sample behind the objective was 0.3 mW.

To separate the Raman signal from the excitation line, an edge filter was used. To achieve Raman Confocality, a 50 mm multi-mode fiberglass was used between the microscope and the Raman spectrometer, where the fiber serves as a pinhole. The Raman spectrometer was equipped with a holographic grating of 600 lines per mm. For the detector, a Newton 970 EMCCD camera (Andor Technology Ltd, United Kingdom) with 1600 x 200 pixels was used, where this configuration allows obtaining a spectral resolution of about 2 cm-1.

To improve the signal-to-noise ratio (S/N), an integration time of roughly 0.1 s per spectrum and pixel was used. For Raman depth scans, 100-pixel x 80-pixel scans were used for covering an area of 50 nm x 40 nm. All data sets were analyzed using cluster analysis and non-negative matrix factorization.

2.2.3.1.2 Scanning electronic microscopy (SEM)

We prepared our sample on Ito-glass, by adding 20 µL of 0.005% PLL-MWCNT which was then evaporated. After that, we fixed the sample on the SEM holder tightly, so it would not move during vacuuming. The images were taken with a constant working distance (WD) of 7.9 mm and electron high tension (EHT) voltage of 5 kV at different magnification powers.

2.2.3.2 Synchronism clips analysis

We evaluated the ability of each condition to engage more cells in the synchronized spikes. The clips were analyzed using a special program called Synicanalysis written in Matlab® designed by George Dressedin (Forschungzentrum Juleich). The implemented parameters are presented in table 7.

Table 7

Final parameters used for clips analysis

Parameter	Value
Number of images to analyze	3000
Number of images to combine	20
The time between two images [sec]	0.0667
%-Threshold for active cells [0-100]	25
Minimum number of active cells	10
Gray value threshold for peaks	1000
Min gray value range for active cells	1000

For statistical analysis, we used GraphPad Prism software, each hole was considered an independent isolate, and each isolate's videos were considered a replicate, the average of replicates was used for analysis, and we compared between the factors [PLL-MWCNT, PLL-ECM] with two parameters first the cellular viability ratio [number of Active cells / Total cell number] and the ratio of synchronism [number of synchronizing Cells/ number of active cells]. To check normality, we used the D'Agostino-Pearson test, then we proceeded with the student's T-test for analysis.

2.2.3.3 Neurite branches analysis

To analyze the neurite branching of cells, a program called BranchAnalysis, written in Matlab®, (Mathworks) was used. The program calculated a mask for all dendrites and a mask for the cell bodies.

To test the significant difference in increasing cell branches between the three factors [PLL-MWCNT/PLL-ECM/PLL], we used GraphPad Prism software for statistical analysis, we set an inclusion range of data between [6-45] branches/cell body as the neuron requires at least 6 branches to function [1 axon and 5 dendrites], and after we reviewed the data, it was found that the program is more precise to scan the branched when it is less than 40. Normality was tested by the D'Agostino-Pearson test then we proceeded with One-way ANOVA for each analysis.

Chapter Three

Results

3.1 Substrate preparation and evaluation

3.1.1 Improvement of MWCNTs dispersion in hydrophilic media

As a result of functionalizing MWCNTs with chitosan and PLL, we observed that both polymers enhanced the dispersion of MWCNTs and yield two black suspensions compared to the pristine-MWCNTs control that precipitate immediately as shown in Figure 2 but it was noticed that the PLL-MWCNTs was more homogenous compared to chitosan-MWCNTs.

Figure 2

Improving the dispersion of MWCNTs dispersion in aqueous media

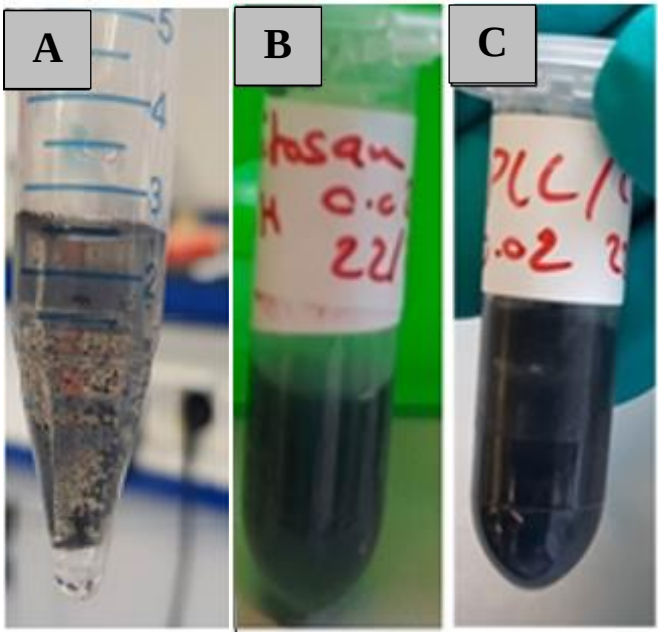

Note. A: pristine-MWCNTs control, B: Chitosan-MWCNTs complex, and C: PLL-MWCNTs complex, showing better dispersion of PLL-MWCNTs and chitosan-MWCNTs compared to pristine form.

Additionally, we found that the chitosan-MWCNTs complex formed a thin layer that detached from the PDMS surface after it was dried, in addition, the surface was rough and thick enough to prevent clear observation through microscopy. This was in contrast to the PLL-MWCNTs complex that formed a black homogenous smooth film, with fair transparency for microscopic visualization. The suspension was also stable after

centrifugation, and no perception was noticed, as a result, we chose the PLL-MWCNTs complex to proceed with.

3.1.2 Interaction between functionalized MWCNTs and PDMS surface

The very first crucial step when developing a substrate for cell growth is to evaluate the distribution of the material on the PDMS surface, especially when dealing with materials at the nanoscale range which might not be observed by inverse microscopes at the micrometer magnification, for this reason, we examined the presence of PLL-MWCNTs films and its homogenous distribution in the beginning with Raman spectroscopy. The analysis yielded spectra of average intensities of the whole surface [PLL-MWCNTs and PDMS polymer] as shown in Figure 3 in green, by overlapping the PDMS and carbon wavelengths spectra we can clearly see the distinctive carbon bands-D band at 1300 rel.1/cm and G band at 1600 rel.1/cm. The analysis focused on areas that look vacant and we still could receive the carbon bands indicating the presence of MWCNTs. By integrating the intensity variations for each band, we obtained a multicolored image as in the following figure, the brighter color is related to the higher intensity of the corresponding band giving an estimate of the composite distribution over the surface, and from the result we had, we can observe a roughly homogenous dispersion of PLL-MWCNTs over the surface.

Figure 3

Investigating the coating adherence and homogenous distribution of PLL-MWCNTs on PDMS surface by Raman spectroscopy

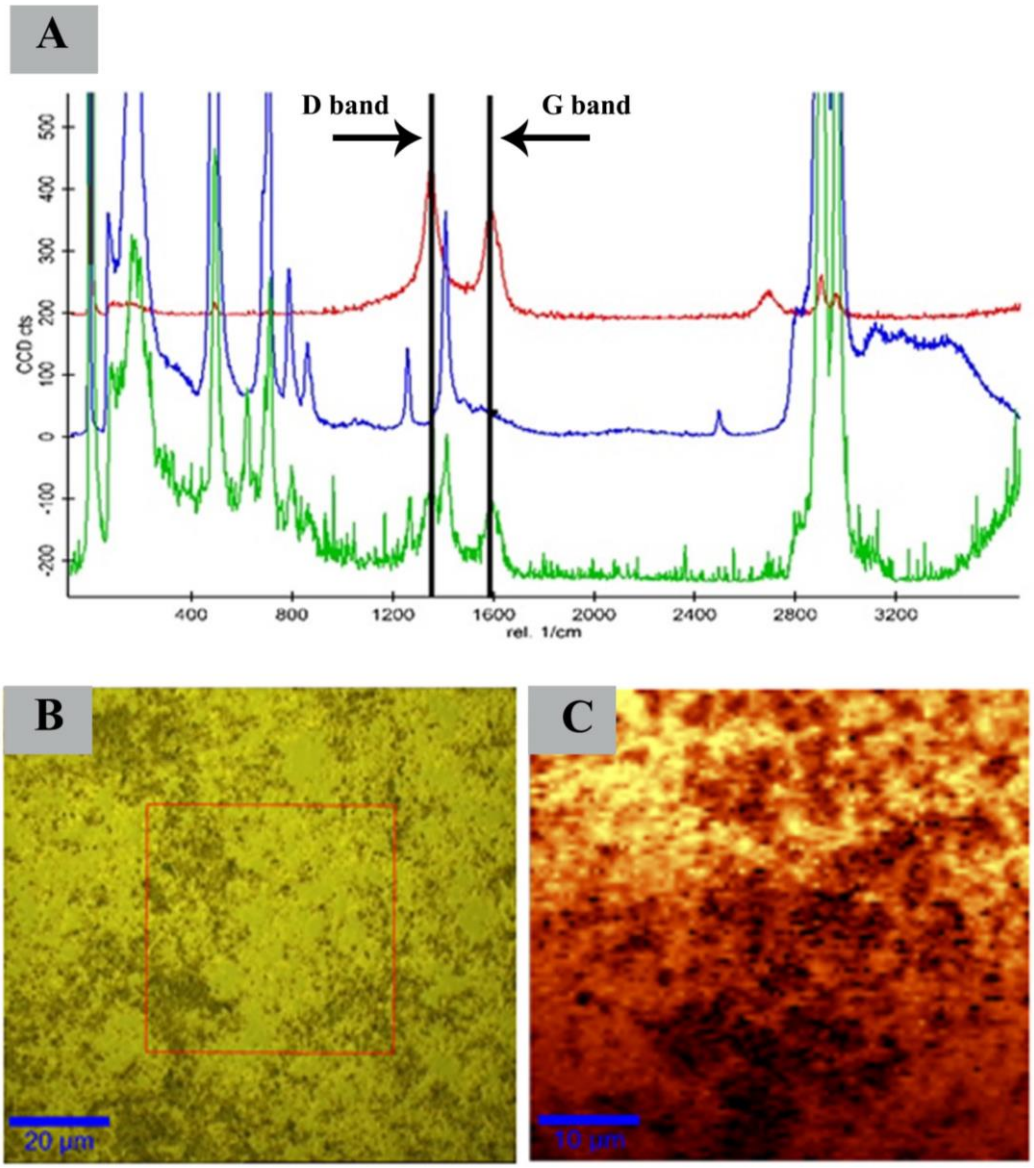

Note. A: The average spectra of the whole surface of both PLL-MWCNTs and PDMS surface are shown in green; blue is the featured wavelength of the PDMS surface, red is the distinctive wavelength of carbon, and the black lines mark the overlapping of D and G bands, which indicates the adherence of MWCNTs coat to the PDMS surface. B: PLL-MWCNTs on PDMS dish microscopic image by Raman upright microscope. C: Integration band intensities of the area inside the red square of image A, brighter yellow color indicates intense signal and more carbon concentration showing the fair homogenous distribution of PLL-MWCNTs on the surface.

The results were supported by the SEM images as shown in figure 4, the PLL-MWCNTs were distributed all over the surface fairly homogenous. The SEM imagining also allowed us to observe MWCNTs characteristics, they were short in length, with different orientations, and fair dispersion on the surface with only a few seen entangled clusters.

Figure 4

Assessment of PLL-MWCNTs distribution on the PDMS surface by SEM

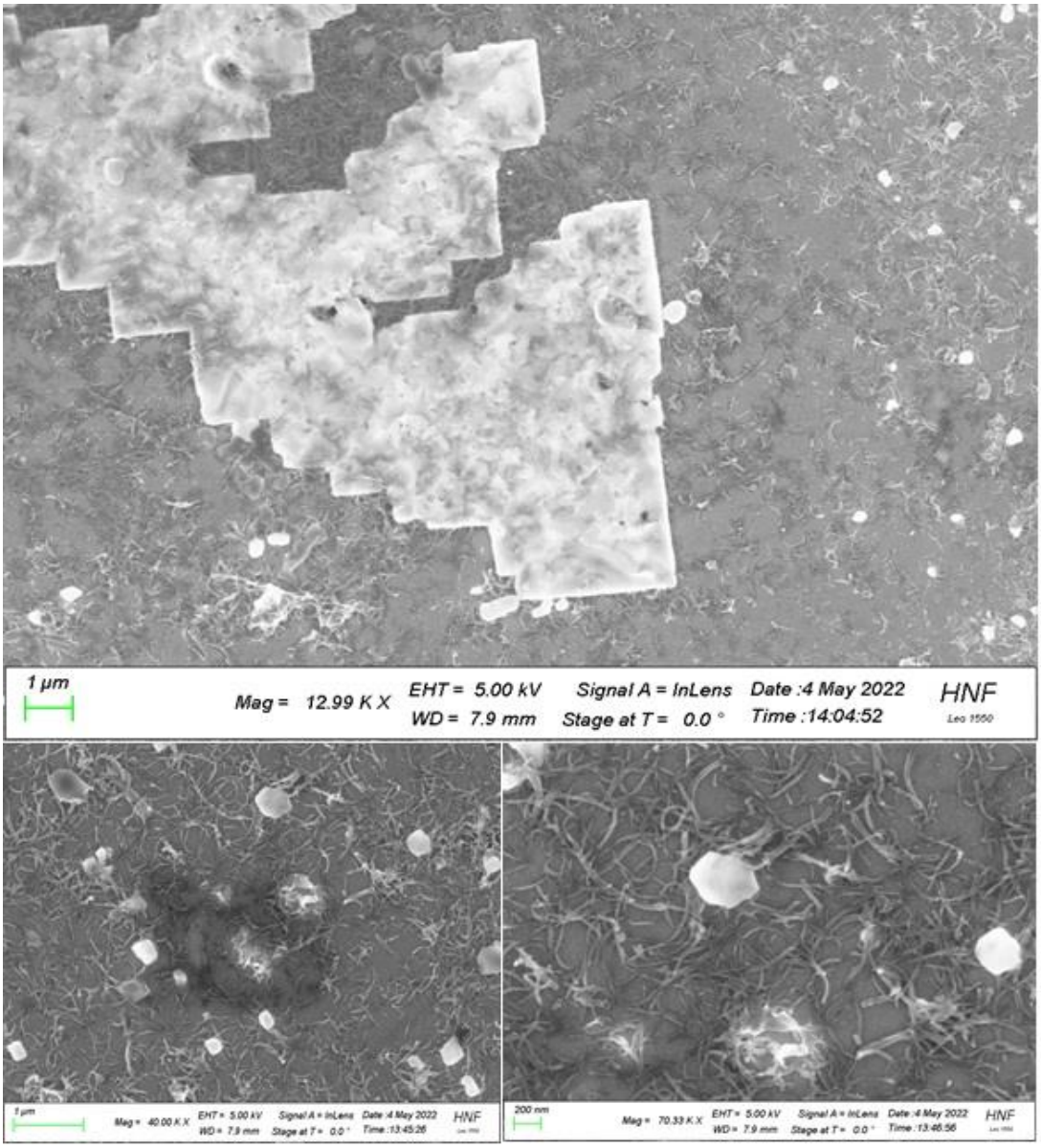

Note. SEM images of PLL-MWCNTs on ITO-glass showing the distribution of PLL-MWCNTs on the surface, the MWCNTs are interconnected, short in length with different orientations. Each image represents a different position of the surface with different magnifications.

3.2 Neuronal adhesion to PLL-MWCNTs and controls substrates

In the first experiments, we tested the cellular adhesion on the PLL-MWCNTs films, and we found that the cells do not adhere to the substrate film directly and they need a further coating for adhesion, probably either the positive charges of PLL were engaged in the functionalization with MWCNTs, or they were hindered reducing the available spots for cellular interaction. For this reason, we added an additional coating layer of 500 µL PLL on the substrate and incubate it overnight, as a result, the neurons were successfully adhering and growing on the substrate. The effect of PLL-MWCNTs composite on cortical neuronal adhesion was tested compared to neurons growing on a PLL alone, as a control and to make sure that the cellular effects we observed were due to the interaction of neurons with PLL-MWCNTs composite and not the additional layer of PLL which was added on top of PLL-MWCNT to enhance the cellular adhesion. We observed a better cell adhesion and more homogenous spreading of cells in all samples growing on PLL-MWCNTs dishes compared to cells growing on PLL dishes where cells tended to form neuronal spheres after a couple of days as shown in figure 5, this observation, in turn, might indicate a stronger cell-surface interaction compared to cell-cell interaction on the PLL-MWCNTs composite, while cells growing on PLL alone favored cell-cell interaction, the formed spheres in PLL dishes will interrupt cellular detection and analysis by software programs, for that reason, we proceeded with PLL-ECM as a control as they were more homogenously distributed compared to PLL dishes.

Figure 5

Growth of cortical neurons on PLL-MWCNT, PLL, and PLL-ECM -coated dishes

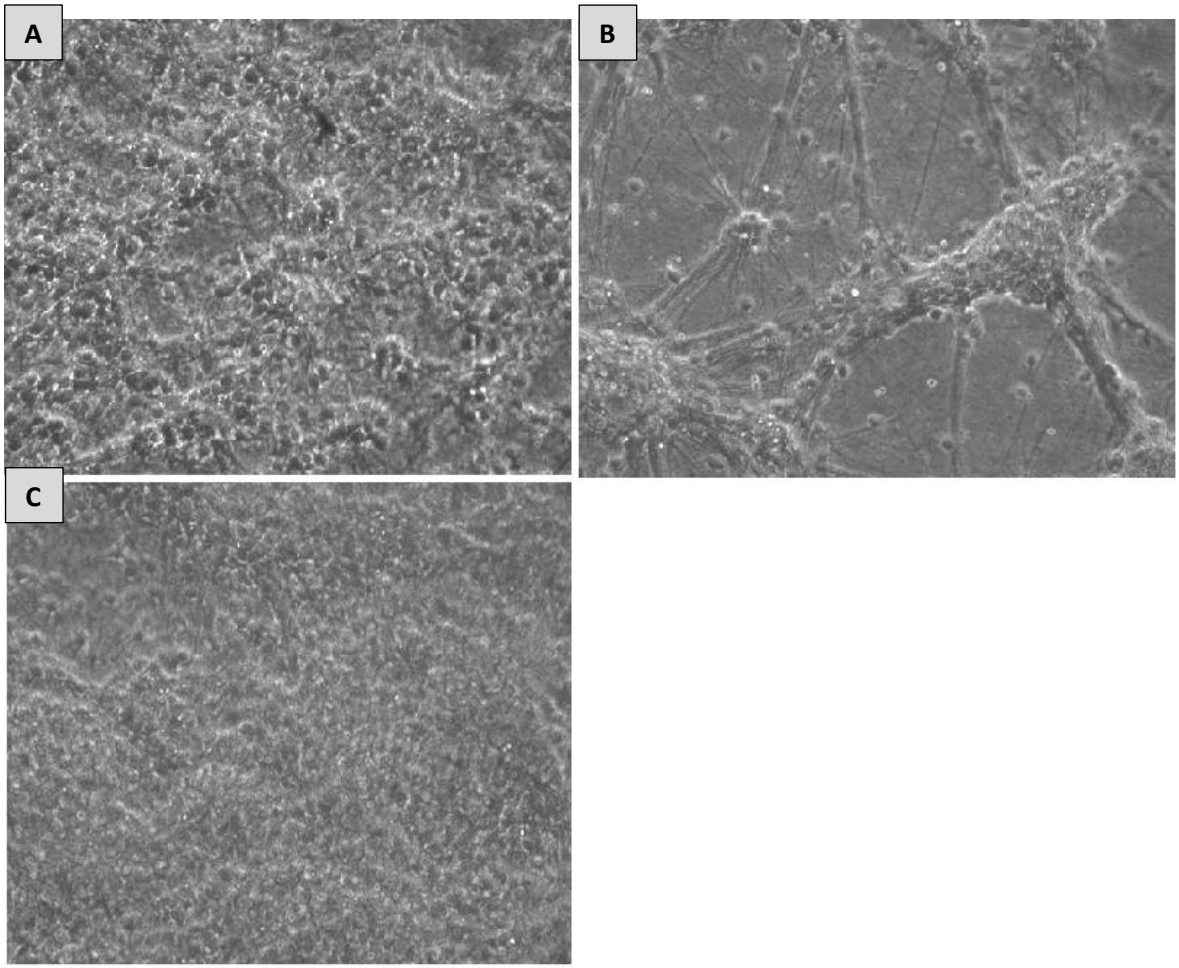

Note. Cortical neurons growing on A: PLL-MWCNTs show the homogenous distribution of neurons, B: PLL alone shows the formation of the spheres, and C: PLL-ECM dishes show the homogenous distribution of cells. This observation indicates better cell-substrate interaction in the PLL-MWCNTs dishes compared to PLL alone. The cells were recorded on day 6 with an inverted microscope air objective 20X.

To determine the best working concentration, we tested three different concentrations to produce three different thicknesses (0.02-0.01-0.005) % w/v of PLL-MWCNTs. We found there is a gradual decrease of cell number survived with thicker PLL-MWCNTs layer, probably with increasing PLL-MWCNTs thickness by drop cast method the surface become more heterogeneous and rough which affects cellular adhesion. The 0.005% concentration showed the best cell adhesion compared to others, which explains the reason for choosing this concentration for our experimental model.

Figure 6

Cortical neurons growth on three different concentrations of PLL-MWCNT substrate Immunostaining of tubulin of cells cultured on PDMS surface coated with three different concentrations PLL-MWCNTs

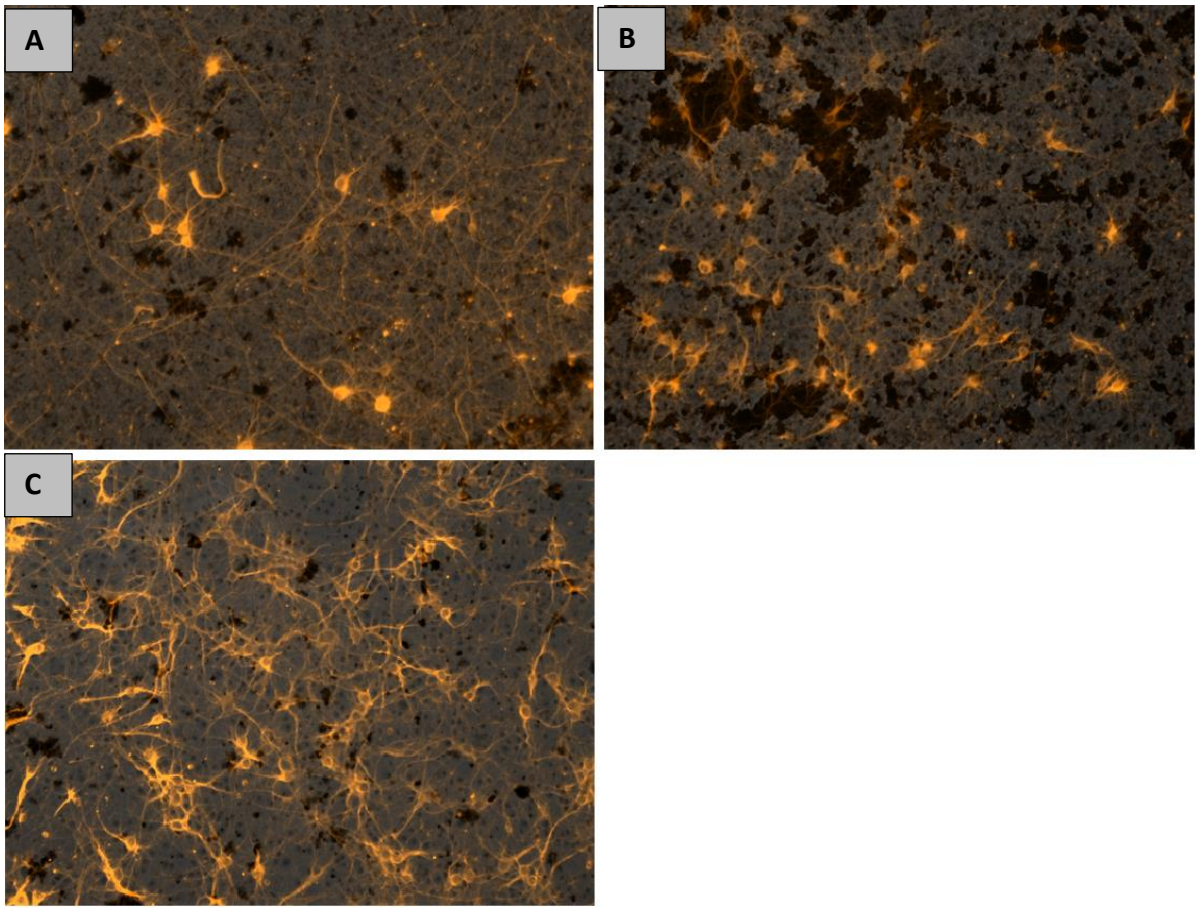

Note. A: 0.02%, B: 0.01%, and C: 0.005%. A gradual decrease in cell viability with increasing PLL-MWCNTs concentration can be observed. Tubulin staining was done on day 6 of culture and visualized with an upright microscope, objective 10X.

3.3 Neuronal synchronism evaluation

We used calcium imagining as an indicator for action potential and circuit functionality, the Syncicanalysis program detects all cells within the image. Therefore, the first 100 images were averaged over time to remove noise in the image. Then this image was smoothed using a gaussian filter (sigma=1). Afterward, a threshold was calculated using Otsu‘s meth. Then all cells are marked and counted as in the following example.

In the next step, the average gray values for each cell label over time were extracted from the images, to reduce noise in the data, 20-time points were averaged, to make sure that all signals have a flat baseline, the slowly varying signal for each cell signal was determined, and subtracted from the original signal.

Then the program detected all active cells and plotted each cell spike per time [sec], now the gray value range (maximum–minimum) for each new cell signal was calculated and cells exceeding a value of 1000, were defined as active cells. For further analysis, only active cells were considered, if less than 10, cells are not active at all, the analysis was not further proceeded. Also, when more than 40% of all detected active cells were synchronizing it would be considered a peak and marked in a red line as in the following figure.

After these steps, the program can identify cells to be dead, active- but not synchronized-, synchronized and can mark each status with a different color as shown in figure 7.

Figure 7

Marking total cell number in a frame of Ca^{+2} staining clips, and automated determination of Cells activity

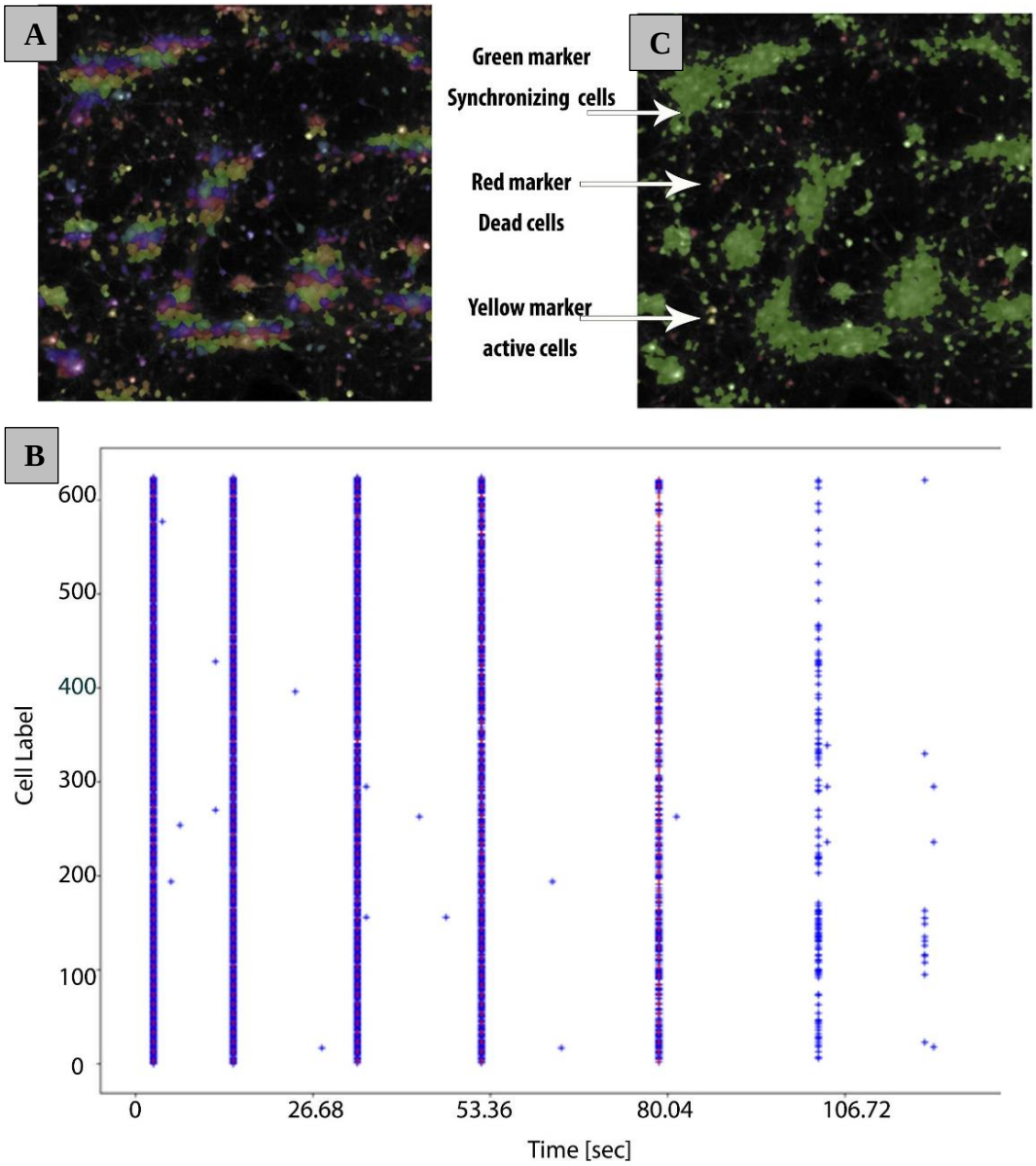

Note. A: PLL-MWCNT dishes frame sample with calcium staining showing a total cell number of 668 cells. The program identifies each cell and marks it with a different color. B: Active cells spike plots per time [sec], the peaks of all calcium signals change the intensities of active cells. The activity of each cell marked in the y-axis is blotted over time, when more than 40% of cells change intensity at the same time point it's considered a synchronized peak and marked in a red line in the middle of plotted marks. C: Cells activity status, the program identifies each cell status and gives it a distinguished color as follows; red: not active cells, yellow: active cells, green: synchronized cells

The program could analyze each clip and yield Excel file plots that calculate the total cell number, the number of active cells, the number of active cells that share the same synchronized peaks, the number of peaks in the clips, and each peak time point. These final were used for the statistical analysis.

Table 8

The Excel file of the SynCanalysis program summarizes the total number of cells, active cells, and synchronized cells in the clip

Total cell number	Total active cell number	Number of synchronized cells	Number of synchronized peaks
668	625	612	5

We compared PLL-MWCNT vs PLL-ECM concerning the effect on neurons circuit. First, we tested the effect of both conditions on cellular viability by calculating the active cell percentage; number of active cells/total cell number, to test which condition supported more viable and active cells. Second, we tested the effect on synchronization to compare which condition engaged more active cells in the synchronized peaks by calculating synchronized cells percentages: number of synchronized cells/active cell number, and we found no significant difference between the two factors which could mean that our substrate didn't negatively influence the synchronization behavior between neuronal cells compared to control dishes as shown in figure 8:

Figure 8

The effect of substrate on the percentage of cellular viability and synchronization

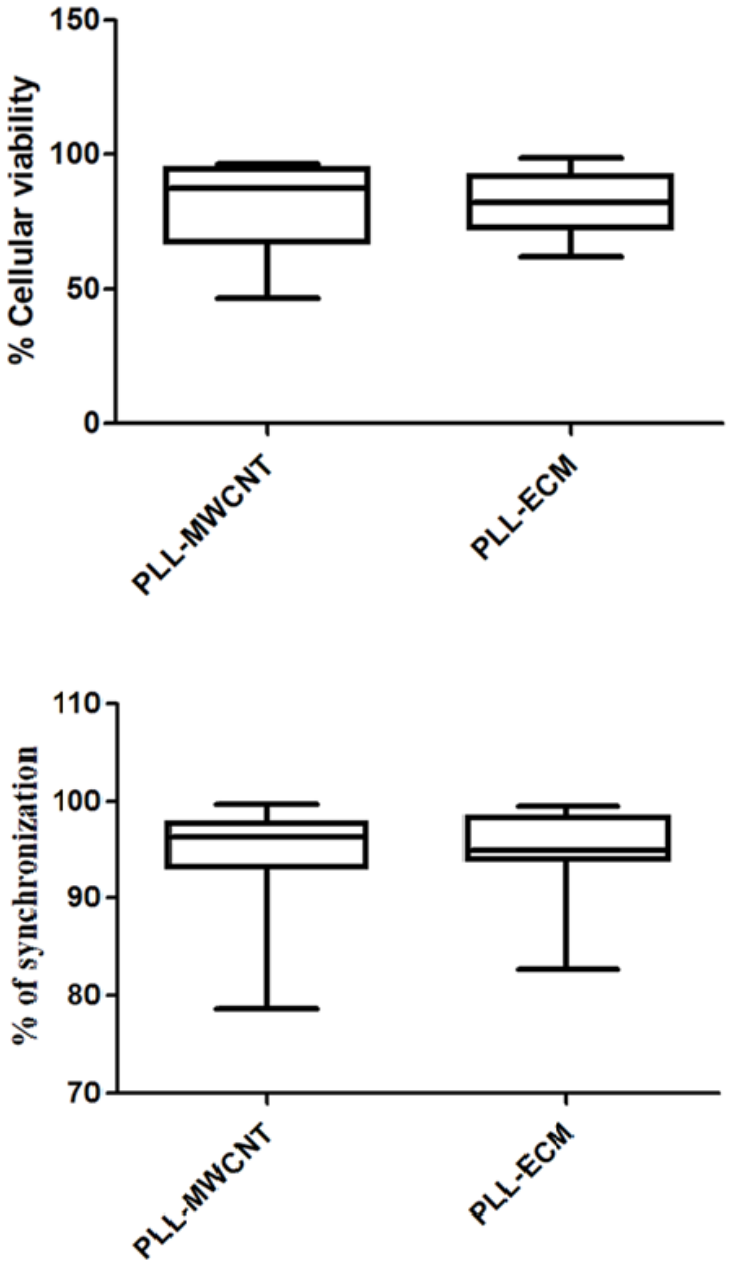

Note. The effect of both substrates on viability Statistical analysis graph between PLL-MWCNT and PLL-ECM conditions in cellular viability percentage [number of active cells/total cell number] resulting in no significant difference with p-value: 0.3045, and the synchronized cell number percentage graph [number of synchronized cells/number of active cells] with p-value: 0.7734 resulting in no significant difference, using student t-test. Number of n=17 for both conditions in both tests.

Neurons grew on PLL-MWCNT substrate with functional circuity and were successful to sustain a similar circuit functionality compared to control PLL-ECM.

3.4 Influence of test substrate on neuritogenesis

Neurite branching is an important parameter to evaluate neurons, as dendrites are the receivers of signals and are highly affected by extracellular cues. The BranchAnalysis program we used, therefore, first smoothed the images using a Gaussian filter. To mask the dendrites, the images were segmented using the mean gray value of the images as a threshold. To reduce artifacts on the mask, some morphological operations were applied to the mask. To mask only the cell bodies that are brighter than the dendrites, the image was again segmented, using the mean gray value plus the standard deviation of the images as a threshold. Again, some morphological post-processing was performed on that mask. The mask for the pure dendrites was created by subtracting the cell body mask from the initial dendrite mask. This mask was then skeletonized. All dendrites connected to a cell body were further analyzed. Since it was not possible to identify which dendrite belongs to which cell, a pseudo-cell area was defined by separating the image into different parts as in the following figure. This was done using the watershed algorithm using the detected cell bodies as a marker. On the skeletonized mask, all branch points were detected, where the part between two points was defined as a branch, and then for each branch, the length and number were calculated. The algorithm was adapted from Li et al(66).

Figure 9

Automated defining of neurite branching in the images by BranchAnalysis software

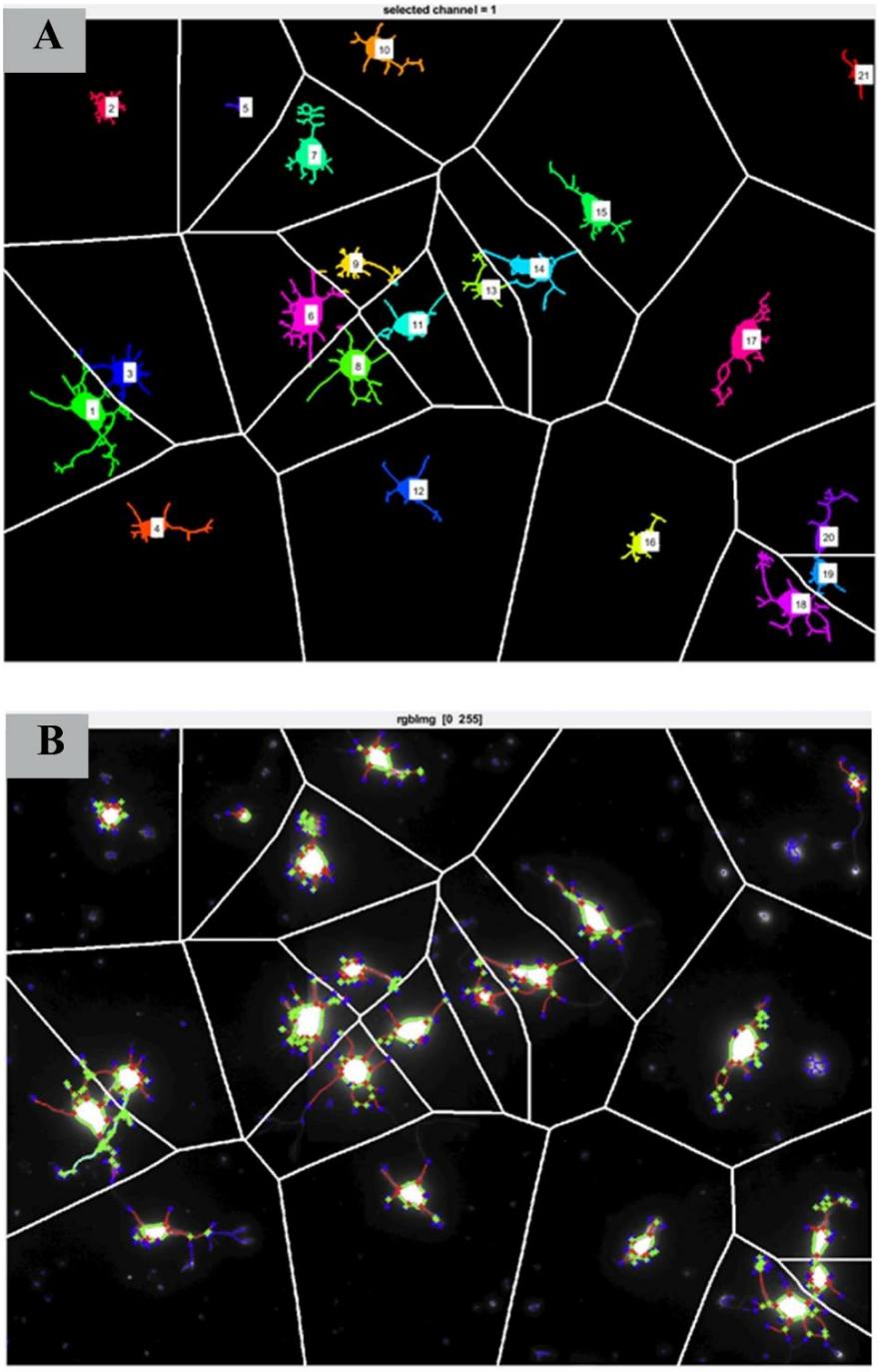

Note. A: PLL-MWCNT dishes sample showing the pseudo area formed to identify each cell separately, we combined channels of actin and tubulin by ImageJ program, and all images were down-scaled by 8 for better analysis. B: Branches identification by determining branches start and end points.

The program yields an Excel sheet for each image, summarizing the parameters we needed in the statistical analysis.

Table 9

The excel calculations show the data as an average of all cells in the image

Number of all branches	Number of cell numbers	Branches per cell body	Sum length per cell body [μm]
419	30	13.967	1221.57

After analyzing over 400 cells of the three factors conditions [PLL-MWCNT, PLL-ECM, and PLL] regarding the number of branches/cell, each cell was considered an independent isolate, with one-way ANOVA test, a significant difference was detected, *p*-value <0.0001 between PLL-MWCNT and the other factors which means that our substrate was able to enhance neuritogenesis as following:

Figure 10

The effect of test substrate on neurite branching

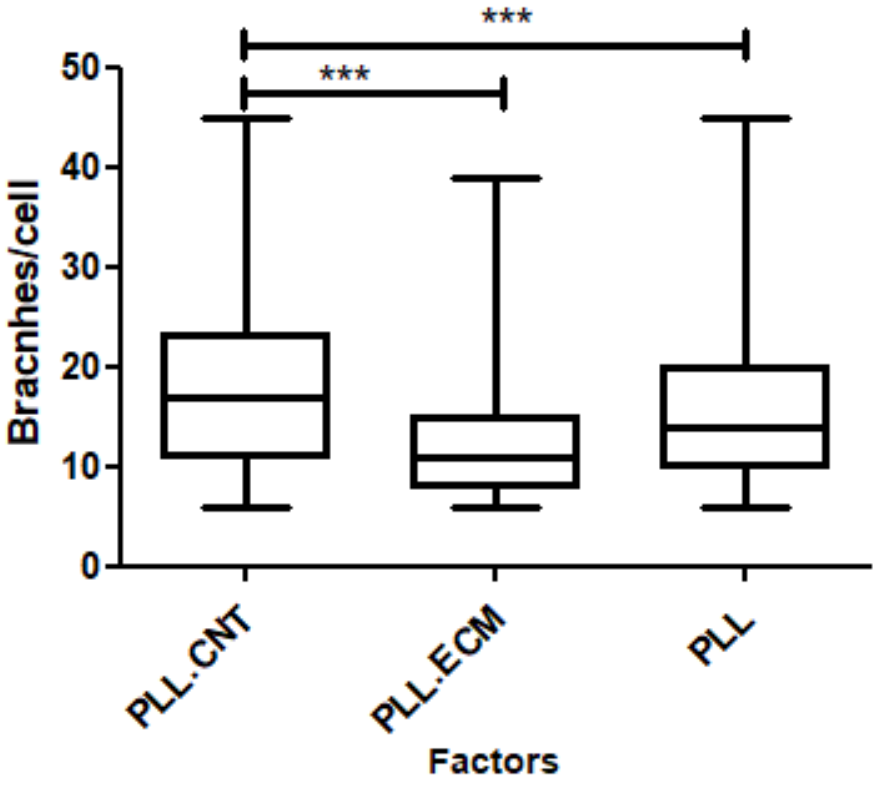

Note. Statistical graphs show the difference between PLL-MWCNTs, PLL-ECM, and PLL conditions for the number of branches/cell, using one way ANOVA test. The p-value was <0.0001indicating a significant difference in cell branches of PLL-MWCNTs compared to other controls. N=619 for PLL, N=516 for PLL-ECM, N=499 for PLL-MWCNTs.

Chapter Four

Discussion

Nerve damage treatment with implantable scaffolds appears to be a promising path, with a limited number of interventions available to treat nerve disorders. However, it is important to put in mind when designing such scaffold some set of requirements such as biocompatibility, electrical conductivity, biodegradability, promote synaptic function and growth in the long run. Hence, material selection has become a crucial step.

Natural polymer-based scaffolds demonstrated excellent bioactivity and maximum cell adhesion, but they are challenging to surface engineer. Carbon nanotubes are playing a positive role in today's science with increasing research papers supporting their neuronal growth and differentiation each day, on the other hand, some restrictions with these systems have emerged, for example, the cytotoxicity of CNT for their favorable tendency for aggregation, and the harsh media of strong acids for disaggregation through covalent bonding causing defects in the side walls of CNTs. In our project, we tended to disaggregate MWCNTs with natural polymer functionalization through more soft conditions, resulting in enhanced dispersion and the formation of PLL-MWCNTs composite, without notable defects observed on the SEM images. This method was published previously in the literature by Ling X *et al* (55), but in our project, we modified some steps, for example, we functionalized the MWCNT with ready-use commercial PLL instead of synthesizing it, and we sonicated both materials directly without treating MWCNTs in HCL, which generated carboxyl group as proven by the FT-IR spectra in their work, we did not test the carboxyl group formation but it is not anticipated as the MWCNTs was not treated by acids through the whole process but it could be generated through sonication method. The process of MWCNTs-PLL composite formation is expected to be wrapping of PLL around the MWCNTs by mechanical sonication or by non-covalent functionalization in case the carboxyl group was generated by sonication through interaction between carboxyl; group and amine groups of the PLL, however, the resulting composite can be dispersed steadily in hydrophilic media due to the hydrogen bonding formed by the amino groups of the PLL (67) causing electrostatic repulsion between MWCNTs tubes.

Scheme 7

PLL functionalization process of MWCNTs Schematic illustration for the expected functionalization of PLL-MWCNTs composite by coating or wrapping of PLL around MWCNTs

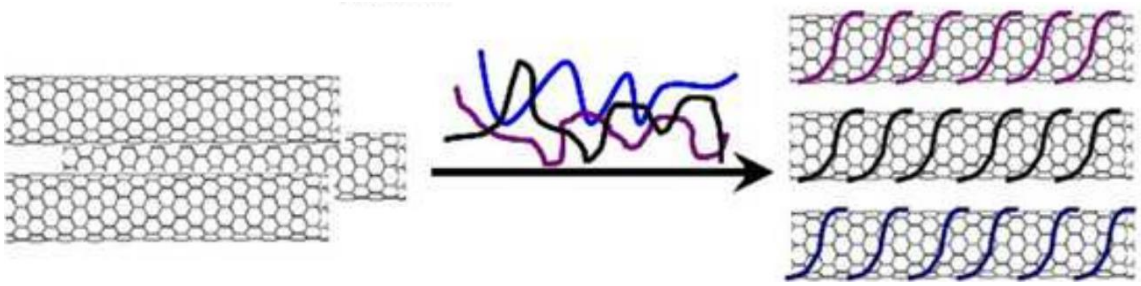

Note. The image was adopted from Ling X et. al., 2014 (55).

Our project is the first to test this kind of composites effects on neurons, at first we expected that the PLL-MWCNTs composite would promote cellular adhesion, but the results were the opposite, and cells needed another layer of PLL to enhance adhesion, maybe that the amino groups of PLL is hindered while wrapping MWCNTs or that they are not enough for a full attachment.

Numerous cell behaviors, such as adhesion, migration, alignment, and differentiation, can be strongly influenced by topographical parameters, including size, shape, and geometric arrangement. To investigate the further effects of PLL-MWCNTs composite nanostructured topography influence on neurons, we decided to test cells at the single and multi-cells scale. The experiments were conducted on a soft PDMS surface with 50 Kpa, to mimic the soft brain environment as closely as possible. At the single-cell scale, we examined the neurite outgrowth by immunohistochemical staining of actin and tubulin, the major neuro-filaments that participate in the formation of filopodia and lamellipodia that are highly influenced by extracellular cues through focal adhesions. We started the process after allowing cells to rest for two days and they were assessed by microscopic images of over 400 cells per each condition at different spots. In our results, we found the mean branches per cell for PLL-MWCNTs was 19.38/cell, for PLL-ECM was 11.57/cell and for PLL was 14.96/cell, the neurite branching for cells on PLL-MWCNTs was significantly higher than the others, which in turn suggest the potential ability of PLL-MWCNTs composite to further enhance neuritogenesis.

The potential mechanism for PLL-MWCNTs composite to trigger dendrites branching through triggering intracellular transduction signal pathways mainly via integrin's mediated focal adhesions (68) that are plasma membrane-associated macromolecules which connect ECM to intracellular actin cytoskeletal filaments (69), and due to this indirect coupling, cells apply forces to sprout under the effect of the biochemical and mechanical cues.

Heterodimeric integrin receptors mediate several cellular interactions with ECM. Integrin clustering causes the recruitment of multiple cellular elements, leading to the formation of the adhesion plaque, a cytoplasmic protein complex. As they grow in size and become more enriched in distinctive proteins including vinculin, focal adhesion kinase, talin, and paxillin, adhesion plaques assemble and mature hierarchically as depicted in scheme 8.

Scheme 8

Focal adhesion assembly The integrin-extracellular binding protein, integrin signaling layer, force transduction layer, and actin regulation layer are all present in the nanoscale structure of focal adhesion

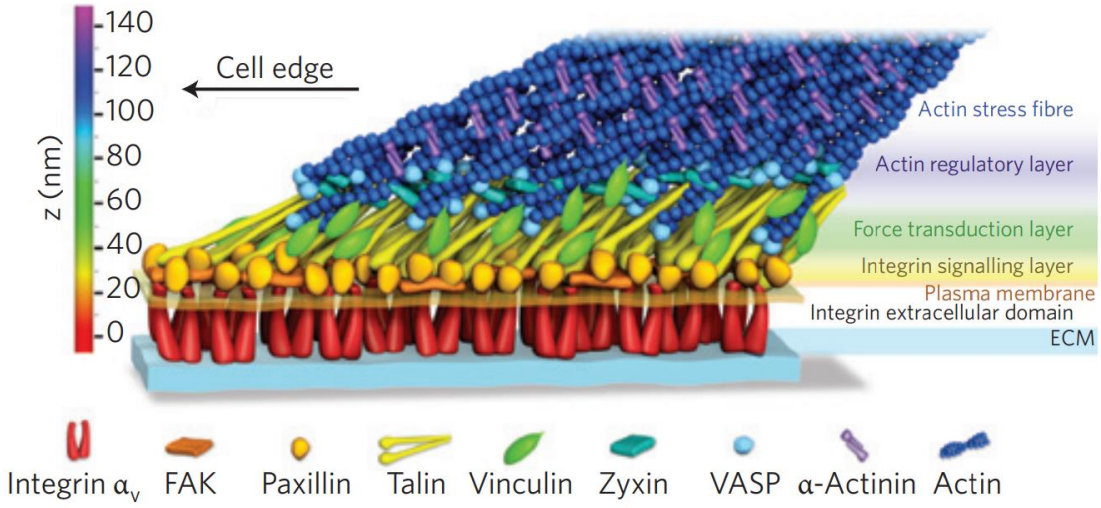

Note. The image was adopted from Dalby MJ et. al., 2014 (70).

A permissive ECM conformation encourages the development of small initial contacts (less than 1 μm) into bigger focal adhesions (FAs). A local equilibrium between the force produced by cell contractility and the ECM response controls the development of FAs. Finally, mature FAs interact with actin microfilaments and can change the shape

of the cell (71, 72), following this, many studies have suggested that the cell-substrate interaction is greatly influenced by structures at the nanoscale rather than the microscale since the focal adhesions sites are in the range of 5-200 nm, so it might that PLL-MWCNTs cylindrical nanoscale tube structure fit preferably with the focal adhesions which in turn increased the triggering of the integrin-ligand complex resulting in actin remodeling, especially that CNT are continuous cylindrical tubes which can direct neurite branch growth alongside. Furthermore, the density of the substrate was found to play a major role in cellular adhesion according to Huang *et al*, who tested osteoblast adhesion on the surface of ligands consisting of arginine, glycine, aspartic acid (RGDs), and they found integrin clusters are enhanced when they increased the intensities of ligand with ligand-ligand spacing less than 70 nm, compared when to surface with lower intensity and interspacing of more than 70 nm between ligands, the cellular adhesion drastically reduced(70) as shown in figure 10. Therefore, the increasing we found in neuron branching and adhesion on PLL-MWCNTs composite might be due to offering interconnected dense topographical cues at the nanoscale. Furthermore, it is expected that MWCNTs increased the surface stiffness compared to the soft PDMS, and according to previous research stated that cortical neurons unlike other types of neurons increased neurite outgrowth significantly on a stiffer substrate (73).

Scheme 9

The interaction between nanoscale topographical cues and neurite sensing

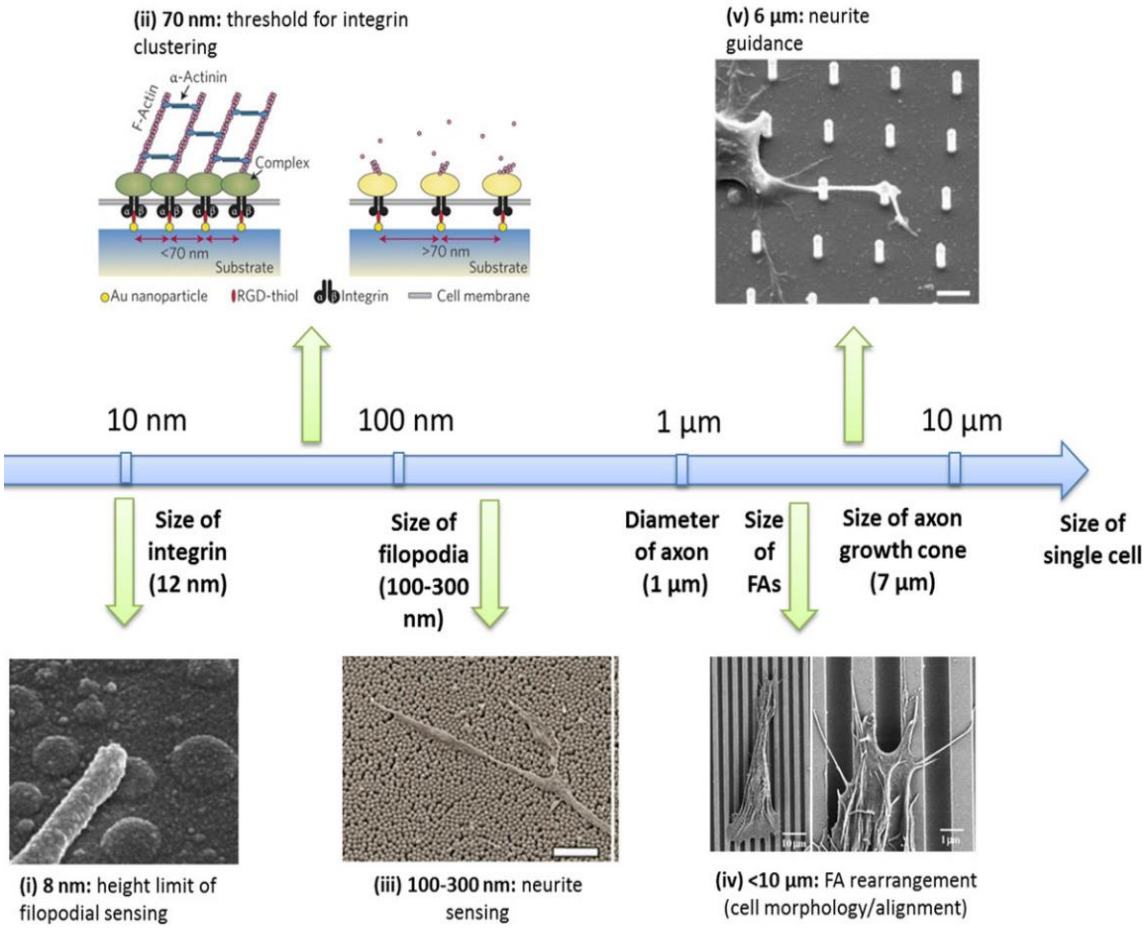

Note. The correlation between topographical cues at the nanoscale and neurite sensing. This figure shows (i) the filopodia can grow high up to 8nm, (ii) this illustration shows the preferred integrin spacing for clustering less than 70 nm, (iii) neurite sensing range, (iv) focal adhesion rearrangement in a size scale less than 10 nm. (v) The longest neurite guidance distance between pillars. The blue lines represent a measuring scale from 10 nm as the size of integrin to 10 µm as the size of a single cell. The image was adopted from Nguyen AT et. al., 2016 (74).

For further investigations on the effect of PLL-MWCNTs composite on neurons, we tested the synchronism behavior at the multi-cell level as a functional neuron not only should maintain sustained growth but also connectivity with other neurons. Neuronal synchronization can be described as a temporal transfer of information between cells correlated at the same time (75, 76), this transfer can be chemical or electrical transmission as clarified in the following scheme, chemical transmission involves the release of neurotransmitters while transferring the information through synaptic cleft from a presynaptic nerve terminal to the following postsynaptic dendrite, whereas, in

the electrical transmission, the information is transferred from cell to another by a cluster of intracellular channels called gap junctions which connects the cytoplasm of adjacent cells, its wide diameter not only allow the transfer of electric currents but also the exchange of metabolites and intracellular signaling molecules including calcium (77, 78).

Scheme 10

Information transmission techniques between neurons

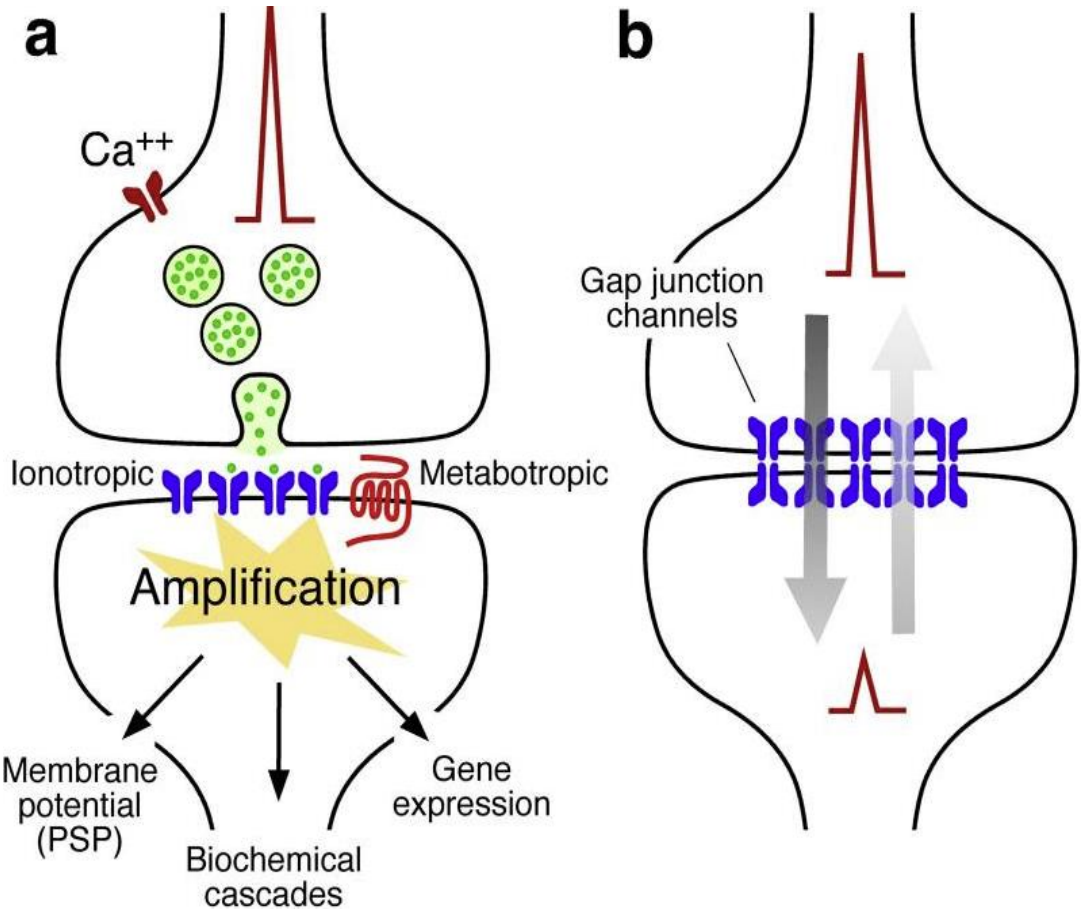

Note. Schematic representation of information transmission between neurons. (a) Chemical transmission by release of neurotransmitters in the synaptic cleft. (b) Electrical transmission shows the gap junctions' connection between two neurons which allows the bi-directional connection. The image was adopted from Pereda AE et. al., 2014 (77).

We used calcium concentration fluctuations as a marker to detect neurons synchronicity, by using an intracellular calcium dye, which increases its fluorescence when binding to calcium.

To evaluate the effect of PLL-MWCNTs composite on neuronal communication between cells, we analyzed the videos by a program that determines the ratio of active cells to the total cell number and the ratio of the synchronizing cells to the active cells number within a video clip, and we found that this composite can sustain a synchronized behavior in about 90% of total active cell number, which was close to that observed at PLL-ECM condition (91.4%). Even though we expected that the increase in the branching of neurons might enhance the cellular communication and increase the total synchronized cells on the PLL-MWCNTs composite but that generated a new question for future work, what if the effects of morphological changes we have detected influenced the neuronal activity by accelerating earlier synchronized spikes than the control.

4.1 Summary

Peripheral and central nervous injuries are still a common and major clinical burden, and treatment is considered a persistent need, especially since the current gold treatment standards such as autologous nerve grafting are occasionally adequate in fully restoring the lost functions, in addition to the burden complications. Nerve tissue engineering has evolved as a new mechanism to construct efficient conduits able to tune neuron growth under the influence of engineered external cues. One of the leading materials that are currently widely investigated is CNTs for their nano-scale topographical cues, and electrical conduction features that could be promising in triggering and directing neuronal branching, but finding an appropriate functionalization that would decrease their toxicity, enhance their dispersion and their neuronal impact is still challenging.

In our project, we have designed a new composite using the combinatory approaches of natural polymers and nanomaterials to enhance MWCNT dispersion in an efficient, simple, and cost-effective way, so that they can serve as a scaffold for neuronal development.

The PLL-MWCNT composite was fairly homogenous and well dispersed on the surface as it was analyzed by Raman spectra and scanning electronic microscopy. We investigated the composite impact on primary isolated rat cortical neurons. Our first observation was the higher adhesion affinity of cells toward PLL-MWCNT composite compared to PLL as a control where cells formed huge spheres which indicated a

stronger cell-substrate interaction compared to cell-cell interactions. Later we tested the morphological changes and the neurite branch formation by staining actin and tubulin the main cytoskeletal filaments by immunocytochemistry between three conditions: PLL-MWCNT. PLL-ECM and PLL alone, we obtained a significant difference in enhancing cellular branching compared to other control conditions, which could be explained mainly by the increase in surface stiffness as well as the exceptional Nano-topography of MWCNT, which is expected to offer extracellular cues in the preferred range for focal adhesion attachment binding indirectly to actin filament causing remodeling in filopodia branching and direction. Finally, we further investigated the influence of this composite on neuronal circuit activity, by analyzing the percentage of synchronized cells between PLL-MWCNT and PLL-ECM as a control, we found that this composite doesn't negatively influence the cell synchronicity and was able to engage cells within the same synchronized spikes similar to PLL-ECM control.

This work is considered basic research towards developing an implantable device for neuronal support aiming to develop a new approach for nerve damage and neurodegenerative diseases.

4.2 Limitations and Recommendations

For the PLL-MWCNT precipitation technique, we used a drop-casting method that cannot provide a full homogenous distribution over the PDMS surface, and lack specific orientation which limited our ability to observe the effect of MWCNT on directing neuronal branching.

For future work, we recommend some ideas to increase our understanding of this composite that we could not perform due to a shortage of time. One of the most important experiments is to analyze the PLL-MWCNT mechanism of interaction and test the presence of possible carboxyl groups' generation in order to be able to determine the type of interaction between PLL and MWCNTs if it is covalent or non-covalent bonding.

Moreover, the PLL-MWCNT should be purified by separating the functionalized form from the excess PLL by ultra-centrifugation, as we conducted an experiment by normal centrifuge but they were not separated, we tried to overcome this obstacle by washing the dishes multiple times with distilled water.

For future work, experiments shall be designed to test the ability of this composite to direct neuronal growth alongside the carbon nanotube by aligning the composite in the same direction, as the MWCNT in our project were with different orientations, and we believe that this composite has an effect on directing neuronal growth but we could not detect this effect so we recommend using an aligned composite.

We also recommend investigating the cellular adhesion in more detail at the molecular level, as better adhesion is reflected in a higher level of gene expression of cell-surface adhesion receptors.

Electrical conductivity is one of the important features of CNT for neurons as they are electrically propagating cells, it will be important to test the composite's conductivity, so it can be used to test the effect of electrical cues for cellular direction and growth.

Importantly, for cellular circuity analysis, we tested relying on previous research in the same institute that detected the best cellular synchronization at day 9 of cellular growth, we recommend testing if the PLL-MWCNT composite might accelerate earlier synchronization between neurons compared to the PLL-ECM condition which might be related to enhancing cellular branching and adhesion.

Lastly, the results we obtained increased our understanding of the PLL-MWCNT effect on neuronal behavior in the 2D model, we recommend proceeding with a 3D model to increase our understanding of the PLL-MWCNT effect on neuronal growth in a more biomimetic model.

List of Abbreviations

Abbreviation	Meaning
µL	Microliter
CAMs	Cell adhesion molecules
Cm	Centimeter
CNS	Central nervous system
CO_2	Carbon dioxide
ECM	Extracellular matrix
EDTA	Ethylene diamine tetra acetic acid
FPS	Frame per second
HBSS	Hank's Balanced Salt Solution
HEPES	4-(2-hydroxyethyl)-1 piperazineethanesulfonic acid
Hrs	Hours
kPa	Kilo Pascal
M	Molarity
MCP-1	Monocyte chemoattractant protein-1
MES	2(N-Morpholino)-ethanesulfonic acid
Mins	Minutes
MWCNTs	Multi-walled Carbon Nanotubes
^{o}C	Degree Celsius
PBS	Phosphate-Buffered Saline
PDMS	Polydimethylsiloxane
PEG	Polyethylene glycol
PFA	Paraformaldehyde
pH	Potential of hydrogen
PLL	Poly-L-lysine
PNS	Peripheral nervous system
Rpm	Round per minute
SEM	Scanning electron microscope
UV	Ultraviolet
v/v	Volume per volume
w/v	Weight per volume

References

[1] Carroll WM. Global, regional, and national burden of neurological disorders, 1990–2016: a systematic analysis for the Global Burden of Disease Study 2016. THE LANCENT neurology 2019;18.

[2] Mo X, Sun B, Wu T, Ei-Hamshary H. 16 - Nanofiber composites in neural tissue engineering. In: Ramalingam M, Ramakrishna S, editors. Nanofiber Composites for Biomedical Applications: Woodhead Publishing; 2017. p. 395-410.

[3] Buchanan TW, Tranel D. Central and peripheral nervous system interactions: from mind to brain to body. International journal of psychophysiology : official journal of the International Organization of Psychophysiology. 2009;72(1):1-4.

[4] Sousa AMM, Meyer KA, Santpere G, Gulden FO, Sestan N. Evolution of the Human Nervous System Function, Structure, and Development. Cell. 2017;170(2):226-47.

[5] Lovinger DM. Communication networks in the brain: neurons, receptors, neurotransmitters, and alcohol. Alcohol research & health : the journal of the National Institute on Alcohol Abuse and Alcoholism. 2008;31(3):196-214.

[6] Chen I LF. Neuroanatomy, Neuron Action Potential: StatPearls; 2021.

[7] Navidmoghaddam A. 2014.

[8] Gordon-Weeks PR. Phosphorylation of Drebrin and Its Role in Neuritogenesis. Advances in experimental medicine and biology. 2017;1006:49-60.

[9] da Silva JS, Dotti CG. Breaking the neuronal sphere: regulation of the actin cytoskeleton in neuritogenesis. Nature reviews Neuroscience. 2002;3(9):694-704.

[10] Tanaka A, Fujii Y, Kasai N, Okajima T, Nakashima H. Regulation of neuritogenesis in hippocampal neurons using stiffness of extracellular microenvironment. PloS one. 2018;13(2):e0191928.

[11] Menna E, Fossati G, Scita G, Matteoli M. From filopodia to synapses: the role of actin-capping and anti-capping proteins. The European journal of neuroscience. 2011;34(10):1655-62.

[12] Flynn KC. The cytoskeleton and neurite initiation. Bioarchitecture. 2013;3(4): 86-109.

[13] Arikkath J. Molecular mechanisms of dendrite morphogenesis. Frontiers in Cellular Neuroscience. 2012;6.

[14] Borst JG, Sakmann B. Calcium current during a single action potential in a large presynaptic terminal of the rat brainstem. The Journal of physiology. 1998;506 (Pt 1)(Pt 1):143-57.

[15] Südhof TC. Towards an Understanding of Synapse Formation. Neuron. 2018;100(2):276-93.

[16] Lilja J, Ivaska J. Integrin activity in neuronal connectivity. 2018;131(12).

[17] Letort G, Ennomani H, Gressin L, Théry M, Blanchoin L. Dynamic reorganization of the actin cytoskeleton. F1000Research. 2015;4.

[18] Tan ZJ, Peng Y, Song HL, Zheng JJ, Yu X. N-cadherin-dependent neuron-neuron interaction is required for the maintenance of activity-induced dendrite growth. Proceedings of the National Academy of Sciences of the United States of America. 2010;107(21):9873-8.

[19] Togashi H, Sakisaka T, Takai Y. Cell adhesion molecules in the central nervous system. Cell adhesion & migration. 2009;3(1):29-35.

[20] Catala M, Kubis N. Gross anatomy and development of the peripheral nervous system. Handbook of clinical neurology. 2013;115:29-41.

[21] Grinsell D, Keating CP. Peripheral nerve reconstruction after injury: a review of clinical and experimental therapies. BioMed research international. 2014;2014:698256.

[22] SUNDERLAND S. A CLASSIFICATION OF PERIPHERAL NERVE INJURIES PRODUCING LOSS OF FUNCTION. Brain. 1951;74(4):491-516.

[23] Conforti L, Gilley J, Coleman MP. Wallerian degeneration: an emerging axon death pathway linking injury and disease. Nature reviews Neuroscience. 2014;15(6):394-409.

[24] Toews AD, Barrett C, Morell P. Monocyte chemoattractant protein 1 is responsible for macrophage recruitment following injury to sciatic nerve. Journal of neuroscience research. 1998;53(2):260-7.

[25] Campbell WW. Evaluation and management of peripheral nerve injury. Clinical neurophysiology : official journal of the International Federation of Clinical Neurophysiology. 2008;119(9):1951-65.

[26] Moattari M, Kaka G, Kouchesfehani H, Sadraie sh, Naghdi M. Comparison of neuroregeneration in central nervous system and peripheral nervous system. Otorhinolaryngology-Head and Neck Surgery. 2018;3.

[27] Vrbova G, Mehra N, Shanmuganathan H, Tyreman N, Schachner M, Gordon T. Chemical communication between regenerating motor axons and Schwann cells in the growth pathway. European Journal of Neuroscience. 2009;30(3):366-75.

[28] Subramanian A, Krishnan UM, Sethuraman S. Development of biomaterial scaffold for nerve tissue engineering: Biomaterial mediated neural regeneration. Journal of biomedical science. 2009;16(1):108.

[29] Shoichet MS TC, Baumann MD, et al. Strategies for Regeneration and Repair in the Injured Central Nervous System. Indwelling Neural Implants: Strategies for Contending with the In Vivo Environment 2008.

[30] Beris A, Gkiatas I, Gelalis I, Papadopoulos D, Kostas-Agnantis I. Current concepts in peripheral nerve surgery. European journal of orthopaedic surgery & traumatology : orthopedie traumatologie. 2019;29(2):263-9.

[31] Gu X, Ding F, Williams DF. Neural tissue engineering options for peripheral nerve regeneration. Biomaterials. 2014;35(24):6143-56.

[32] Jun Li GL. Cell Transplantation for Spinal Cord Injury: A Systematic Review. Bio Med Research International 2012.

[33] Schmidt CE, Leach JB. Neural tissue engineering: strategies for repair and regeneration. Annual review of biomedical engineering. 2003;5:293-347.

[34] Clements IP, Munson JM, Bellamkonda RV. Chapter II.6.14 - Neuronal Tissue Engineering. In: Ratner BD, Hoffman AS, Schoen FJ, Lemons JE, editors. Biomaterials Science (Third Edition): Academic Press; 2013. p. 1291-306.

[35] Jain D, Mattiassi S, Goh EL, Yim EKF. Extracellular matrix and biomimetic engineering microenvironment for neuronal differentiation. Neural regeneration research. 2020;15(4):573-85.

[36] Amini S, Salehi H, Setayeshmehr M, Ghorbani M. Natural and synthetic polymeric scaffolds used in peripheral nerve tissue engineering: Advantages and disadvantages. Polymers for Advanced Technologies. 2021;32(6):2267-89.

[37] Doblado LR, Martínez-Ramos C, Pradas MM. Biomaterials for Neural Tissue Engineering. Frontiers in Nanotechnology. 2021;3.

[38] Zhang BG, Quigley AF, Myers DE, Wallace GG, Kapsa RM, Choong PF. Recent advances in nerve tissue engineering. The International journal of artificial organs. 2014;37(4):277-91.

[39] Kafa H, Wang JT, Al-Jamal KT. Current Perspective of Carbon Nanotubes Application in Neurology. International review of neurobiology. 2016;130: 229-63.

[40] Negri V, Pacheco-Torres J. Carbon Nanotubes in Biomedicine. 2020;378(1):15.

[41] Wick P, Manser P, Limbach LK, Dettlaff-Weglikowska U, Krumeich F, Roth S, et al. The degree and kind of agglomeration affect carbon nanotube cytotoxicity. Toxicology letters. 2007;168(2):121-31.

[42] Zaib Q, Ahmad F. Optimization of Carbon Nanotube Dispersions in Water Using Response Surface Methodology. ACS omega. 2019;4(1):849-59.

[43] Kharlamova MV, Paukov M, Burdanova MG. Nanotube Functionalization: Investigation, Methods and Demonstrated Applications. Materials. 2022;15(15):5386.

[44] Hwang J-Y, Shin US, Jang W-C, Hyun JK, Wall IB, Kim H-W. Biofunctionalized carbon nanotubes in neural regeneration: a mini-review. Nanoscale. 2013;5(2): 487-97.

[45] Marrina Flichakova VS. Single-walled carbon nanotubes: structure, properties, applications, and health & safety 2021. Available from: https://tuball.com/articles/single-walled-carbon-nanotubes.

[46] Fraczek-Szczypta A. Carbon nanomaterials for nerve tissue stimulation and regeneration. Materials Science and Engineering: C. 2014;34:35-49.

[47] Fabbro A, Bosi S, Ballerini L, Prato M. Carbon nanotubes: artificial nanomaterials to engineer single neurons and neuronal networks. ACS chemical neuroscience. 2012;3(8):611-8.

[48] Fabbro A, Prato M, Ballerini L. Carbon nanotubes in neuroregeneration and repair. Advanced Drug Delivery Reviews. 2013;65(15):2034-44.

[49] Olakowska E, Woszczycka-Korczyńska I, Jędrzejowska-Szypułka H, Lewin-Kowalik J. Review paperApplication of nanotubes and nanofibres in nerve repair. A review. Folia Neuropathologica. 2010;48(4).

[50] Mattson MP, Haddon RC, Rao AM. Molecular functionalization of carbon nanotubes and use as substrates for neuronal growth. Journal of molecular neuroscience : MN. 2000;14(3):175-82.

[51] Hu H, Ni Y, Montana V, Haddon RC, Parpura V. Chemically Functionalized Carbon Nanotubes as Substrates for Neuronal Growth. Nano Letters. 2004;4(3):507-11.

[52] Zhang X, Prasad S, Niyogi S, Morgan A, Ozkan M, Ozkan CS. Guided neurite growth on patterned carbon nanotubes. Sensors and Actuators B: Chemical. 2005;106(2):843-50.

[53] Jang MJ, Namgung S, Hong S, Nam Y. Directional neurite growth using carbon nanotube patterned substrates as a biomimetic cue. Nanotechnology. 2010;21(23):235102.

[54] Malarkey EB, Fisher KA, Bekyarova E, Liu W, Haddon RC, Parpura V. Conductive Single-Walled Carbon Nanotube Substrates Modulate Neuronal Growth. Nano Letters. 2009;9(1):264-8.

[55] Ling X, Wei Y, Zou L, Xu S. Functionalization and dispersion of multiwalled carbon nanotubes modified with poly-l-lysine. Colloids and Surfaces A: Physicochemical and Engineering Aspects. 2014;443:19-26.

[56] Ahsan SM, Thomas M, Reddy KK, Sooraparaju SG, Asthana A, Bhatnagar I. Chitosan as biomaterial in drug delivery and tissue engineering. International journal of biological macromolecules. 2018;110:97-109.

[57] Bąk M, Gutkowska ON, Wagner E, Gosk J. The role of chitin and chitosan in peripheral nerve reconstruction. Polimery w medycynie. 2017;47(1):43-7.

[58] Gregory H, Phillips JB. Materials for peripheral nerve repair constructs: Natural proteins or synthetic polymers? Neurochemistry international. 2021;143:104953.

[59] Wahba MI. Enhancement of the mechanical properties of chitosan. Journal of biomaterials science Polymer edition. 2020;31(3):350-75.

[60] Zheng M, Pan M, Zhang W, Lin H, Wu S, Lu C, et al. Poly (α-l-lysine)-based nanomaterials for versatile biomedical applications: Current advances and perspectives. Bioactive materials. 2021;6(7):1878-909.

[61] Miranda I, Souza A. Properties and Applications of PDMS for Biomedical Engineering: A Review. 2021;13(1).

[62] Murphy MC, Huston J, 3rd, Jack CR, Jr., Glaser KJ, Manduca A, Felmlee JP, et al. Decreased brain stiffness in Alzheimer's disease determined by magnetic resonance elastography. Journal of magnetic resonance imaging: JMRI. 2011;34(3):494-8.

[63] Abraham J-A. Influence of cyclic mechanical strain on tissues of the central nervous system: Rheinische Friedrich-Wilhelms-Universität Bonn; 2020.

[64] Available from: https://www.aatbio.com/resources/application-notes/cal-520-reg-cal-590-trade-and-cal-630-trade-calcium-detection-reagents.

[65] Butler HJ, Ashton L, Bird B, Cinque G, Curtis K, Dorney J, et al. Using Raman spectroscopy to characterize biological materials. Nature protocols. 2016;11(4):664-87.

[66] Li W, Tang QY, Jadhav AD, Narang A, Qian WX, Shi P, et al. Large-scale topographical screen for investigation of physical neural-guidance cues. Sci Rep. 2015;5:8644.

[67] Yu B, Wang X, Ding L, Han M, Guo Y. Hydrophilic Natural Polylysine as Drug Nanocarrier for Preparation of Helical Delivery System. Pharmaceutics. 2022;14(11): 2512.

[68] Ye L, Ji H, Liu J, Tu C-H, Kappl M, Koynov K, et al. Carbon Nanotube–Hydrogel Composites Facilitate Neuronal Differentiation While Maintaining Homeostasis of Network Activity. Advanced Materials. 2021;33(41):2102981.

[69] Fischer RS, Lam P-Y, Huttenlocher A, Waterman CM. Filopodia and focal adhesions: An integrated system driving branching morphogenesis in neuronal pathfinding and angiogenesis. Developmental Biology. 2019;451(1):86-95.

[70] Dalby MJ, Gadegaard N, Oreffo ROC. Harnessing nanotopography and integrin–matrix interactions to influence stem cell fate. Nature Materials. 2014;13(6): 558-69.

[71] Simitzi C, Ranella A, Stratakis E. Controlling the morphology and outgrowth of nerve and neuroglial cells: The effect of surface topography. Acta Biomaterialia. 2017;51:21-52.

[72] Lanoue V, Cooper HM. Branching mechanisms shaping dendrite architecture. Developmental Biology. 2019;451(1):16-24.

[73] Athamneh AI, Suter DM. Quantifying mechanical force in axonal growth and guidance. Front Cell Neurosci. 2015;9:359.

[74] Nguyen AT, Sathe SR, Yim EK. From nano to micro: topographical scale and its impact on cell adhesion, morphology and contact guidance. Journal of physics Condensed matter : an Institute of Physics journal. 2016;28(18):183001.

[75] Lodi M, Della Rossa F, Sorrentino F, Storace M. Analyzing synchronized clusters in neuron networks. Scientific Reports. 2020;10(1):16336.

[76] imofeev I BM, Seigneur J, et al. Neuronal Synchronization and Thalamocortical Rhythms in Sleep, Wake and Epilepsy. Jasper's Basic Mechanisms of the Epilepsies 2012.

[77] Pereda AE. Electrical synapses and their functional interactions with chemical synapses. Nature reviews Neuroscience. 2014;15(4):250-63.

[78] Bennett MVL, Zukin RS. Electrical Coupling and Neuronal Synchronization in the Mammalian Brain. Neuron. 2004;41(4):495-511.

جـامعـــة النجاح الوطنية
كليـــة الدراســـات العليـــا

تطوير ركائز تعتمد على الانابيب النانوية الكربونية متعددة الجدران المفعلة بروابط غير تساهمية لدعم نمو الخلايا العصبية مخبريا

إعداد
راما سهم هنداوي

إشراف
د. نعيم كتانه
د. محي الدين العسالي

قدمت هذه الرسالة استكمالا لمتطلبات الحصول على درجة الماجستير في علم الادوية، من كلية الدراسات العليا، في جامعة النجاح الوطنية، نابلس- فلسطين.

2023

تطوير ركائز تعتمد على الانابيب النانوية الكربونية متعددة الجدران المفعلة بروابط غير تساهمية لدعم نمو الخلايا العصبية مخبريا

إعداد

راما سهم هنداوي

إشراف

د. نعيم كتانه

د. محي الدين العسالي

الملخص

الخلفية: تعتبر الاصابات العصبية السبب الرئيسي الأول للإعاقات والسبب الرئيسي الثاني للوفيات على مستوى العالم، مما يضيف عبئًا كبيرًا على الاقتصاد الاجتماعي. تم تطوير العديد من التدخلات لعلاج إصابات الأعصاب، واحدة من اهم المعايير الذهبية هي الخياطة العصبية عندما تكون ممكنة، بالاضافة الى زرع الأعصاب الذاتي، على الرغم من نتائجهم الواعدة، الا ان التعافي الوظيفي من الإصابات المزمنة لا يزال يمثل تحديًا. نتيجة لذلك، ظهرت هندسة الأنسجة العصبية لإيجاد حلول مبتكرة. في مشروعنا، هدفنا إلى تطوير نمو الخلايا العصبية من خلال تعزيز تشتت الأنابيب النانوية الكربونية متعددة الجدران MWCNT في الاوساط المائية واستخدامها كركيزة بنائية للخلايا العصبية .

الأهداف: يهدف مشروعنا إلى اختبار تأثير الركيزة البنائية المكونة من الانابيب النانوية متعددة الجدران (MWCNT) على وظائف الخلايا العصبية، من خلال تعزيز تشتت MWCNT أولاً وتشكيل ركيزة تسمح بنمو الخلايا العصبية.

المنهجية: من اجل تعزيز تشتت الMWCNT في الاوساط المائية، قمنا بربطه باستخدام ال-poly-l lysine وال chitosan عن طريق الصوتنة، وترسيبه على سطح البوليمر PDMS، ثم عزلت الخلايا العصبية من ادمغة اجنة الجرذان من المنطقة القشرية، ثم قمنا بتحليل الركيزة بواسطة اطياف الرامان

والمجهر الالكتروني (SEM). تم اختبار تزامن التشابك العصبي عن طريق صبغة الكالسيوم وتم تحليل مقاطع الفيديو المسجلة بشكل اكبر بواسطة برنامج SyincAnalysis، وتم تحليل النتائج احصائيا عن طريق Student T test، وتم تحليل مورفولوجيا الخلايا العصبية عم طريق صبغ الاكتين والتوبولين واللذان يعدان من اهم الخيوط الهيكلية الرئيسية في تشكل الخلية العصبية، وتم تحليل الصور بواسطة برنامج خاص لفحص عدد التشعبات في الخلية العصبية. وتم تحليل النتائج احصائيا من خلال One-way-ANOVA.

النتائج والاستنتاجات: عزز ال PLL تشتت MWCNT بشكل أفضل من ال chitosan. بالنسبة للمزامنة العصبية، قمنا باختبار الركيزة النانو كربونية مقابل PLL-ECM، ولم نجد فرقًا كبيرًا بين نسبة عدد الخلايا النشطة ونسبة الخلايا المتزامنة بين الحالتين مما يشير الى عدم تاثير الركيزة النانوكربونية بشكل سلبي. بالنسبة للمورفولوجيا العصبية وجدنا ان الركيزة النانوكربونة زادت من التشعبات العصبية للخلية بشكل مؤثر مقارنة ب PLL وPLL-ECM. يعتقد ان تكون هذه التاثيرات نتيجة سطح الركيزة النانوي الذي قد يفضل للارتباط الخلوي.

الكلمات المفتاحية: انابيب كربونية نانوية، بولي ال لايسين، شيتوزان، تزامن عصبي، مورفولوجيا عصبية، هندسة انسجة عصبية، ركيزة خلوية.